

# The 1804 Alborán Seismic Series: Search for the Source

Yolanda de Pro-Díaz \*<sup>1</sup>, Jose J. Martínez-Díaz <sup>1-2</sup>, Carolina Canora-Catalán <sup>3</sup>

<sup>1</sup>Department of Geodynamics, Stratigraphy and Paleontology, Universidad Complutense de Madrid, Madrid, Spain, <sup>2</sup>Instituto de Geociencias (CSIC, UCM), <sup>3</sup>Department of Geology and Geochemistry, Universidad Autónoma de Madrid, Cantoblanco, Spain

**Author contributions:** *Conceptualization:* Y. de Pro-Díaz. *Data Curation:* Y. de Pro-Díaz. *Formal Analysis:* Y. de Pro-Díaz. *Funding Acquisition:* Y. de Pro-Díaz, J. J. Martínez-Díaz, C. Canora-Catalán. *Investigation:* Y. de Pro-Díaz, J. J. Martínez-Díaz, C. Canora-Catalán. *Methodology:* Y. de Pro-Díaz. *Project Administration:* J. J. Martínez-Díaz. *Supervision:* J. J. Martínez-Díaz, C. Canora-Catalán. *Validation:* J. J. Martínez-Díaz, C. Canora-Catalán. *Visualization:* Y. de Pro-Díaz. *Writing – original draft:* Y. de Pro-Díaz. *Writing – review & editing:* Y. de Pro-Díaz, J. J. Martínez-Díaz, C. Canora-Catalán.

**Abstract** Linking historical earthquakes with the faults that caused them is crucial for seismic hazard assessment. Historical documentation describing the effects of an earthquake is a useful information source, from which we can compile the observed intensity field of the earthquake. In this work, we use intensity data from the catastrophic 1804 Alborán earthquake (south of Iberia) along with intensity simulations and coseismic stress transfer analysis to search for this earthquake's seismic source. We build intensity simulations for each fault proposed as a potential source, and compare these simulations with the intensity field. We also propose the possibility of the Alborán 1804 earthquake triggering the Dalías earthquake (European macroseismic intensity ( $I_{EMS-98}$ ) IX), which occurred seven months after, and analyze stress transfer between the possible sources of both earthquakes. Our results point to a conjunct rupture of the northern Al-Idrissi Fault segment and the North–South Faults as the most likely source for the Alborán earthquake.

**Resumen** Relacionar los terremotos históricos con sus fallas responsables es crucial para las evaluaciones de peligrosidad sísmica. Una fuente de información sobre estos terremotos es la documentación histórica que describe sus efectos, a partir de la cual se puede recopilar el campo de intensidad observada del terremoto. En este trabajo utilizamos los datos de intensidad del terremoto de Alborán de 1804 (al sur de Iberia) junto con simulaciones y análisis del cambio de esfuerzos cosísmico para buscar su falla responsable. Construimos simulaciones de intensidad para las distintas fallas propuestas como fuentes y las comparamos con el campo de intensidad. También proponemos un posible *triggering* entre el terremoto de Alborán y el terremoto de Dalías ( $I_{EMS-98}$  IX) ocurrido siete meses después, y analizamos la posible transferencia de esfuerzos entre las posibles fuentes de ambos terremotos. Nuestros resultados apuntan a una ruptura conjunta del segmento norte de la Falla de Al-Idrissi con las Fallas Norte-Sur como la fuente más probable del terremoto de Alborán.

**Non-technical summary** Knowing as best as we can the faults that cause earthquakes and how they behave over time helps in designing earthquake-resistant structures, which avoids earthquake damage. Studying the effects caused by historical earthquakes is one way to achieve this. We use felt data recorded from the 1804 Alborán earthquake (south of Spain) to search for the fault that most likely caused this earthquake. We recreate the felt earthquake shaking intensity by trying out different possible faults as sources and compare the hypothetical shaking intensity caused by each scenario with the historically documented intensity. The recreation that best fits the historical observations will also be the one built on the most similar source model to the actual earthquake source. We also propose the Alborán earthquake could have triggered another event (the Dalías earthquake), which occurred nearby seven months later and explore this possibility. We link the Alborán earthquake with a combined rupture of the northern part of Al-Idrissi Fault and the nearby North–South Faults.

## 1 Introduction

In active but slow-to-moderate moving plate boundaries, such as the diffuse limit between Africa and the Iberian Peninsula, active faults may show recurrence periods longer than the instrumental record. In these regions, associating historical earthquakes with their causative fault and including accurate historical earthquake data in seismic hazard assessment (SHA) studies can make a difference when considering whether

or not a particular fault is active and might rupture in the future. The importance of addressing faults as seismogenic sources in SHA studies and extend back their known seismic history beyond the instrumental record has been rising in the recent years (e.g., [Ambraseys and Jackson, 1998](#); [Basili et al., 2008](#); [Caputo et al., 2015](#); [Gómez-Novell et al., 2020](#)). Paleoseismology, which studies geological evidence of past earthquakes, is one way to achieve this; however, there are seismically active areas where paleoseismological analysis cannot be performed. As [McCalpin and Nelson \(1996\)](#) noticed, this might happen because of several dif-

Production Editor:  
Andrea Llenos  
Handling Editor:  
Vitor Silva  
Copy & Layout Editor:  
Tara Nye

Signed reviewer(s):  
Joao Duarte

Received:  
October 22, 2024  
Accepted:  
June 11, 2025  
Published:  
July 15, 2025

\*Corresponding author: ypro@ucm.es

ferent reasons:

- The structures that expose an earthquake occurrence (such as fault scarps, fault scars, or liquefaction structures) never formed in the first place due to the site's geological conditions.
- The structures did form, but high erosion rates immediately dismantled them.
- Human activity has destroyed these structures.
- The structures are located in an area that is not easily accessible (such as offshore or in a densely forested area).

In the particular case of blind offshore faults, geophysical exploration might also give some insights on their location, and widespread turbiditic deposits may provide information on their activity. However, this kind of oceanographic data is not yet available for every region of seismic interest. When paleoseismic and oceanographic studies cannot be conducted, another approach to address whether or not a fault is active and extend its history past the instrumental record is to analyze historically recorded earthquake effects. Documents such as newspapers, personal diaries, letters to the authorities, and reconstruction bills provide researchers with plenty of information about earthquakes that occurred in historical times (Muñoz Clares et al., 2012; Murphy Corella, 2019; Teves-Costa and Batlló, 2010). In some cases, historical documents also preserve descriptions of geological evidence even after the structure itself has disappeared due to erosion or anthropogenic activities (Huerta et al., 2015; Murphy Corella, 2019). Damage and effects reported in these documents can be graded using modern intensity scales, such as the European Macroseismic Scale (EMS-98; Grünthal, 1998) or the Environmental Seismic Intensity scale (ESI-07; Michetti et al., 2007). With reports of earthquakes' effects on multiple sites, we can compile the intensity field of historical earthquakes.

It has been noted in many studies how seismic intensity correlates reasonably well with strong ground-motion parameters, such as peak ground acceleration (PGA) and peak ground velocity (PGV) (Trifunac and Brady, 1975; Wald et al., 1999; Atkinson and Wald, 2007; Delavaud et al., 2009). Because of this correlation, several authors have developed ground-motion-to-intensity conversion equations (GMICES), which allow one to estimate the intensity caused by a certain ground-motion value and vice versa (e.g., Kaka and Atkinson, 2004; Atkinson and Kaka, 2007; Tselenitis and Danciu, 2008; Worden et al., 2012; Caprio et al., 2015). Additionally, different authors have also developed ground-motion models (GMM), which calculate the ground motion at a certain location considering a certain seismic source (e.g., Campbell, 2003; Ambraseys et al., 2005; Akkar and Bommer, 2010; Abrahamson et al., 2014; Campbell and Bozorgnia, 2014; Pezeshk et al., 2018; Akkar et al., 2013). Plenty of research has also been done on the effect that an earthquake causes on the local stress state and how it can influence the

occurrence of future events, usually using the analysis of Coulomb failure static stress change ( $\Delta$ CFS) (e.g., Okada, 1992; Harris, 1998; Stein, 1999, 2003; King et al., 1994).

Through the combined use of GMM, GMICE, and/or  $\Delta$ CFS, and knowing the parameters of a seismic source, we can build simulations of the effects that this source can induce on building and terrain, as well as estimate static stress changes in its vicinity. We can also use this approach to look into the past and search for the source of historical earthquakes when the causative fault is unclear and no other evidence is found. The assumption is as follows: If we build a simulation that matches the observed effects, the seismic source on which we built that simulation could be considered as the possible source of the earthquake. Using different variations of this approach, the source of many historical earthquakes has been searched for in previous works. Fracassi and Valensise (2007) compared the pattern of damage distribution during the seismic crisis of 1456 in Italy with the regional tectonic structures to search for earthquake sources that had not been addressed before. Silva et al. (2017) used the correlation between PGA and intensity, as well as a trial-and-error modeling procedure, to search for the source of the 1755 Lisbon, the 1829 Torre Vieja, and the 1863 Huércal-Overa earthquakes. A similar procedure was followed by Rodríguez-Pascua et al. (2017) in their research on the 1884 Arenas del Rey earthquake. Canora et al. (2021), after locating the earthquake surface rupture of the 1531 Lisbon earthquake in a trench, estimated the rupture length by building different seismic scenarios and comparing them with the observed intensity field. Lozos (2016) also combined paleoseismic data with historic damage reports and rupture modeling to study the 1812 California earthquake. Griffin et al. (2018) combined the use of GMM and GMICE with a search algorithm to investigate the source of several historical earthquakes east of the Sunda Arc. Hough and Graves (2020) used hybrid broadband simulations to study different possible scenarios for the 1933 Long Beach earthquake. Other authors, instead of working with intensity or ground motions, have modeled the stress transfer caused by different possible earthquake sources and compared it with the local seismicity after an earthquake of interest to search for its source. Such is the case of the Catalan seismic series of 1427–1428 (Perea, 2009), the 2001 El Salvador earthquake (Canora et al., 2010), and the 2019 Jijel and 2014 Ziyama earthquakes (Yelles-Chaouche et al., 2021).

In this work, we search for the most likely source of the Almería earthquake of 13<sup>th</sup> January 1804, also known as the 1804 Alborán earthquake, which caused significant damage on both the Spanish and Moroccan coasts, as well as at several inland locations. The greatest damage occurred in the building stock from the province of Granada and especially Almería (Murphy Corella, 2019). This earthquake has been assigned  $M_w$  6.3–6.7 by different authors, mostly based on the damage (Martínez Solares and Mezcua Rodríguez, 2002; Posadas et al., 2006; Mezcua et al., 2013). To investigate its source fault, we use a methodology based on simula-

tions of hypothetical earthquake shaking intensity. We estimate the intensity values that could be caused if the earthquake had originated on different possible faults, and then we compare these simulated intensities with the historical intensities in search of the scenario that better fits the observed data. We use a methodology proposed by de Pro-Díaz et al. (2022, 2023) and incorporate a new extra step using  $\Delta$ CFS analysis to better constrain the results.

## 2 Neotectonic and seismic context

### 2.1 The Betics and Alborán Sea area

The study area is located south of the Iberian Peninsula (Figure 1), and it includes the Alborán Sea and the eastern part of the Betic Cordillera. The Betic Cordillera, also known as the Betics, is an ENE–WSW orogen located south of the Iberian Peninsula (Figure 1). During the neotectonic period (Late Miocene to Present), tectonic activity in the Eastern Betics is dominated by the convergence between Iberia and Nubia plates (DeMets et al., 2010; Serpelloni et al., 2007; Nocquet and Calais, 2004). The study area is located in the Eastern Betics where a transpressional stress field with NNW–SSE shortening has been dominant during the Quaternary (Echeverría et al., 2015). This strain regime is consistent with the kinematics of the largest active faults in this area (Martínez-Díaz et al., 2012). One of the most important fault systems in the Alborán Sea is the Trans-Alborán Shear Zone (De Larouzière et al., 1988), a sigmoidal, NE–SW, transpressive fault zone formed mainly by left-lateral strike-slip faults, and reverse faults on the northern sector (Silva et al., 1993). The Trans-Alborán Shear Zone also reaches inland and connects with the Betics. Its continental part is called the Eastern Betics Shear Zone, which has been largely studied (e.g., Ferrater et al., 2016, 2017; Herrero Barbero, 2021; Insua-Arevalo et al., 2015; Martín-Banda et al., 2016; Ortuño et al., 2012).

The Carboneras Fault (CF) is one of the major faults of the Trans-Alborán Shear Zone, and part of its trace runs south of the epicentral area of the Alborán earthquake (Figure 1) (Gràcia et al., 2006; Moreno Mota, 2011; Moreno et al., 2015, 2016; Álvarez-Gómez et al., 2023). Another major fault near the epicentral area is the Al-Idrissi Fault (AIF), a currently growing, NE–SW oriented, subvertical, left-lateral strike-slip fault which has been related to the 2016 Al Hoceima earthquake ( $M_w$  6.3) (Ammar et al., 2007; Gràcia et al., 2019; Lafosse et al., 2020; Martínez-García et al., 2011; Martínez-García et al., 2013; d’Acromont et al., 2014; Álvarez-Gómez et al., 2016). This earthquake could have also triggered the seismic series of 2021–2022 near Al Hoceima, although the latter series has not been related to the AIF but with a parallel unmapped structure (Lozano et al., 2025; Perea et al., 2022). Both the CF and AIF are considered not only active and seismogenic, but also potentially tsunamigenic (Álvarez-Gómez et al. (2023); Gómez de la Peña et al. (2022)). Connected to the AIF to the north there is a wide left-lateral shear zone known as the North–South Fault system (NSF); recent research

suggests it is a currently developing extension to the north of the AIF (Canari et al., 2024; Gràcia et al., 2019). West of the northern sector of the AIF, but with a par-

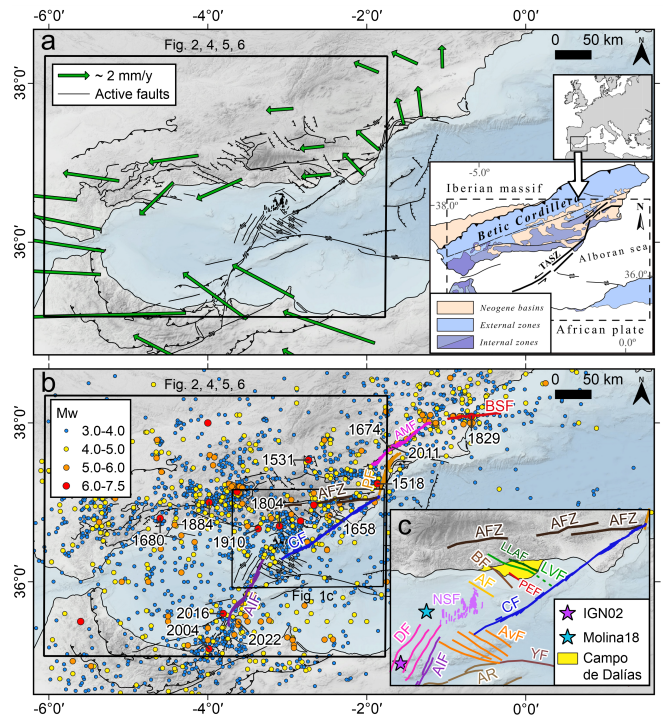


**Figure 1** Seismotectonic context for the study region. Inset modified from Herrero-Barbero et al. (2021). Seismic catalog from the Instituto Geográfico Nacional and Universidad Complutense de Madrid (ICN-UGM, 2013), represented as dots with the dates of the main earthquakes. a) GNSS velocities are represented as green arrows, from Palano et al. (2015). b) Fault traces from the Quaternary Active Faults of Iberia (QAFI) database (García-Mayordomo et al., 2012) and other sources (Canari et al., 2024; Gràcia et al., 2019; Perea et al., 2018; Moreno et al., 2016; Estrada et al., 2017) are represented as black lines, with the main faults of the Eastern Betics Shear Zone and Trans-Alborán Shear Zone highlighted in color. c) Detail of the block between the Alpujarras Fault Zone and the Carboneras Fault. CF: Carboneras Fault. AFZ: Alpujarras Fault Zone. PF: Palomares Fault. AMF: Alhama de Murcia Fault. BSF: Bajo Segura Fault. AIF: Al-Idrissi Fault. AF: Adra Fault. AvF: Averroes Faults. DF: Djibouti Faults. LVF: Loma del Viento Fault. NSF: North–South Faults. AR: Alboran Ridge. PEF: Punta Entinas Fault. LLAFF: Llano del Águila Fault. YF: Yussuf Fault. IGN02: epicenter for the 1804 Alborán earthquake located by Martínez Solares and Mezcuá Rodríguez (2002). Molina18: epicenter for the 1804 Alborán earthquake located by Molina et al. (2018).

allel strike to it and showing similar left-lateral strike-slip kinematics is the Djibouti Fault (DF) (Canari et al., 2024; Gràcia et al., 2019). East of this sector of the AIF is the Averroes Fault (AvF) and its associated North Averroes Faults. The AvF is a WNW–ESE fault with a main right-lateral strike-slip component, although it becomes a normal fault towards the western tip line (Canari et al., 2024; Perea et al., 2018; Moreno et al., 2016; Estrada et al., 2017). Further north in the continent, the Alpujarras Fault Zone is also an important structure in this area: an E–W, strike-slip, right-lateral cor-

ridor composed of several faults, some of which have been active in the Quaternary (Echeverría et al., 2015; Martínez-Martínez, 2006; Sanz de Galdeano et al., 1985, 2020). The Alpujarras Fault Zone and the CF are the northern and south-eastern limits of a complex crustal block which is divided in smaller, rotating blocks delimited by oblique (normal-strike-slip) faults trending NW–SE (Martínez-Díaz and Hernández-Enrile, 2004). The smaller NW–SE faults control several Neogene basins, such as the Campo de Dalías (Figure 1). Among these NW–SE faults are the Loma del Viento Fault (LVF) (Pedrera et al., 2012; Murphy Corella, 2019; Martínez-Díaz, 1999; Marín-Lechado et al., 2005; García-Mayordomo et al., 2012), the Llano del Águila Fault (LLAF) (Molins-Vigatà et al., 2022), the Adra Fault (AF), the Balanegra Fault (BF) (Gràcia et al., 2006, 2012; Martínez-Díaz and Hernández-Enrile, 2004; Marín-Lechado et al., 2010; Sanz de Galdeano et al., 2020) and the Punta Entinas Fault (Gràcia et al., 2006, 2012; García-Mayordomo et al., 2012), which all share normal-dextral kinematics.

## 2.2 The 1804 Almería seismic series

In 1804, two seismic series occurred in the Campo de Dalías area and its offshore proximity (Figure 1), one in January and the other in August. These series are usually known as the 1804 Almería seismic series. The mainshock of the January series, which is the focus of this work, occurred on the 13<sup>th</sup> and was felt at several locations along both the south Iberian Peninsula's and north African coasts (Espinár Moreno, 1994; Murphy Corella, 2019). The mainshock of the August series occurred on the 25<sup>th</sup> near the city of Dalías (Figure 2), and its most likely source appears to be a conjunct rupture of the Loma del Viento Fault (LVF) and the Llano del Águila Fault (LLAF) (de Pro-Díaz et al., 2023).

The 1804 Almería seismic series were extensively researched by Murphy Corella (2019). This author recovered historical documents describing the effects of the earthquakes and their consequences in the affected areas and analyzed these records in order to assign EMS-98 intensity values to each site. The author also included data from geological effects—such as hydrogeological anomalies, scarps, and fissures, and others—to assign ESI-07 intensity values. Although this author focused mainly on the 25<sup>th</sup> August earthquake, which was the most damaging of the series, he also addressed the 13<sup>th</sup> January earthquake in his analysis, as well as the strongest aftershocks in both the January and August series. In the following paragraph, we translate and summarize some of Murphy Corella (2019)'s research regarding the 13<sup>th</sup> January earthquake, for which he compiled an intensity dataset of 26 points, which when combined with the macroseismic intensity field of Martínez Solares and Mezcua Rodríguez (2002), makes a total of 30 intensity data points (Figure 2). This is the observed intensity field that we use in our analysis.

The most affected town was Motril ( $I_{EMS-98}$  VII) (Figure 2), where the sea was described to withdraw 22 varas (~18 m), and the earthquake caused “ruins and two deaths”, it being the only site with confirmed casu-

alties for the 13<sup>th</sup> January earthquake. Records addressing the effects in Motril also include the arrival time of what can be identified as the different seismic waves: an east to west “perpendicular movement” at 5:53 pm, “trepidation” after 14–16 seconds for about 4–5 seconds, and then more than 20 seconds of “strong undulation movement”x with “underground noise”. Because of the seismological interest of these records, this event was known as the Motril earthquake for some time. Motril's citizens camped outside town in fear of the shaking until the aftershocks stopped by the end of February. Records from the coastal town of Adra ( $I_{EMS-98}$  VII) (Figure 2) describe how the earthquake was felt by the population, as well as a “disturbance in the sea, which was shaken with noisy movement, which completely ceased” after each shock of the January series. In the towns of Berja and Dalías ( $I_{EMS-98}$  VI-VII) (Figure 2), historical records (Murphy Corella, 2019) describe damage in several buildings after the January mainshock, including the four churches in these two towns. Fear of this earthquake and its subsequent aftershocks drove the people of these two localities to camp outside town for a whole month until the so called “tremors” stopped, and damage could be fixed during spring season. Certain buildings were severely damaged in Roquetas ( $I_{EMS-98}$  VI). Records from the city of Almería's municipal archive ( $I_{EMS-98}$  VI) (Figure 2) report extensive damage to the whole building stock, although there were no casualties. The earthquake was also felt in Málaga ( $I_{EMS-98}$  V-VI) (Figure 2), where “startled people occupied the streets and squares”, as well as in several cities far from the epicentral area, like Sevilla, Melilla (Figure 2) or even Madrid, more than 400 km north of the epicentral area (Murphy Corella, 2019). These are the most known sites where the earthquake was felt and caused damage, but its effects are reported in more localities (Figure 2). A more detailed translation of the reported effects at these sites and some others can be found in Table S1 of the supplement.

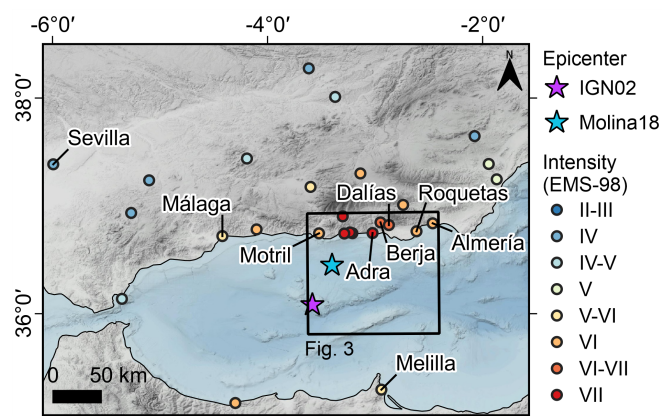


**Figure 2** Intensity field of the Alborán earthquake of 13<sup>th</sup> January 1804 compiled by Murphy Corella (2019) and combined with Martínez Solares and Mezcua Rodríguez (2002). IGN02: epicenter estimated by Martínez Solares and Mezcua Rodríguez (2002). Molina18: epicenter estimated by Molina et al. (2018).

Two different locations have been proposed for the

epicenter using intensity data: 36.083 °N, 3.583 °W by Martínez Solares and Mezcua Rodríguez (2002), estimated from the center of the highest intensity area with a previous and less rich dataset; and 36.45 °N, 3.40 °W by Molina et al. (2018), who used Murphy Corella (2019)'s data and also considered the reported S–P arrival time difference from Motril (Figure 2). As stated before, different authors have proposed magnitudes of  $M_W$  6.3–6.7 for this earthquake also using intensity data for their estimations (Martínez Solares and Mezcua Rodríguez, 2002; Posadas et al., 2006; Mezcua et al., 2013). As for the seismic source, Espinar Moreno (1994), Martínez Solares and Mezcua Rodríguez (2002), Molina et al. (2018), and Murphy Corella (2019) all agree on an offshore source based on the damage distribution at both the Spanish and Moroccan coasts, as well as the tsunami reports (IGN, 2024). Murphy Corella (2019) proposed the offshore extension of the LVF as a possible source for this earthquake, although this is not the closest fault to the epicenters estimated by Martínez Solares and Mezcua Rodríguez (2002) and Molina et al. (2018) (Figures 2 and 3). No evidence of surface rupture has been found inland so far for this earthquake, which may support the offshore source hypothesis.

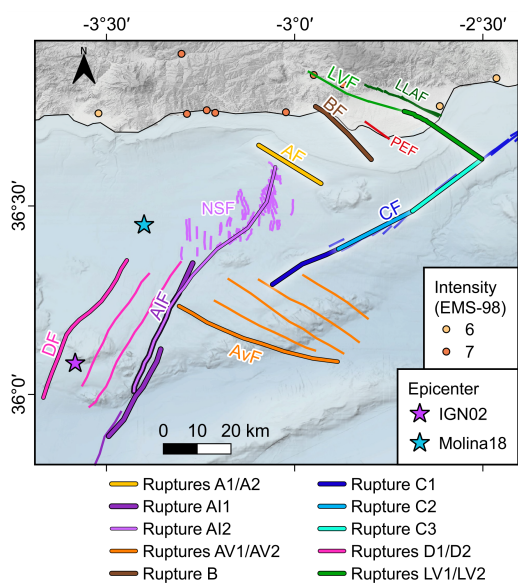


**Figure 3** Fault segments chosen as candidate faults for the 1804 Alborán earthquake. Fault parameters are presented in Table 1. Candidate faults are named as follows: A1, A2: Adra Fault ruptures; AI1 and AI2: Al-Idrissi Fault ruptures; AV1, AV2: Averroes Fault ruptures; B: Balanegra Fault rupture; C1, C2, C3: Carboneras Fault ruptures; D1 and D2: Djibouti Fault ruptures; LV1, LV2: Loma del Viento Fault ruptures.

### 3 Methodology

In this work, we have used the seismic scenario method proposed by de Pro-Díaz et al. (2022, 2023) for constraining the earthquake source through the use of seismic scenarios and the observed intensity field. We have also added an extra step using Coulomb stress transfer analysis to be used as an additional criterion to rank the pre-

ferred scenarios. The methodology is composed of four steps:

**1. Search for possible sources.** The original methodology in de Pro-Díaz et al. (2023) uses Gasperini et al. (1999, 2010)'s method and their Boxer software to calculate the most likely area of the surface where the seismic source might be located (called “boxer”). The boxer is compared with known active faults to search for faults that partially or totally overlap, which are considered as possible sources for the earthquake (“candidate faults” henceforth). However, the spatial distribution of intensity data in an offshore earthquake might compromise the boxer results, so this approach cannot be applied to the 1804 Alborán earthquake. In this work, candidate faults are selected among known active faults documented by other authors, as well as the ones included in the QAFI database by García-Mayordomo et al. (2012) (updated 2022). Candidate faults for this earthquake must be mainly offshore, close to the epicenter and/or the highest shaking intensity data points, and long enough to produce at least an  $M_W$  6.3, the minimum magnitude proposed by independent authors for this earthquake.

**2. Seismic scenarios.** We build seismic scenarios for each one of the candidate ruptures using the Open-Quake software (Pagani et al., 2014). OpenQuake takes  $M_W$ , geometry, position and rake of the rupture, as well as position of the hypocenter as input data. Using a ground-motion model (GMM), it produces a regular grid of points over the study area, each containing estimates of ground motion—in this work, peak ground acceleration (PGA) and peak ground velocity (PGV). Since nowadays most GMMs take into account soil types through  $V_{S30}$  (time-averaged shear-wave velocity in the upper 30 m of crust), we also input the  $V_{S30}$  model of Allen and Wald (2007). Then, using ground-motion-to-intensity conversion equations (GMICES), we estimate the intensity values that would be caused by the simulated ground motion. In this work, we tested two GMMs: Campbell and Bozorgnia (2014) and Akkar and Bommer (2010). The Campbell and Bozorgnia (2014) GMM was recommended for this area by Quirós Hernández (2017) and has shown good results before with similar methodologies (de Pro-Díaz et al., 2023). It was built using data from the PEER NGA-West2 database (Bozorgnia et al., 2014), which contains seismic records from magnitude 3.3 to 7.5–8.5 earthquakes with a wide variety of focal mechanisms in California and all over the world. Although normal faulting is slightly less represented than reverse and strike-slip faulting. The Akkar and Bommer (2010) GMM, on the other hand, was built using data from this study region and the rest of the Mediterranean with a magnitude range of 5 to 7.6 and significantly less representation of reverse faulting than normal or strike-slip faulting. As for the GMICE, we tested Worden et al. (2012) and Caprio et al. (2015). Worden et al. (2012) showed good results before in de Pro-Díaz et al. (2023), although it was developed using data mainly from North America, while Caprio et al. (2015) was developed using data from the Mediterranean region and includes regional corrections. Each scenario is then compared to the observed intensity field using this equation:

Rupture	Strike (°)	Dip (°)	Rake (°)	Area (km <sup>2</sup> )	Length (km)	Fault Origin	SD (km)	Epicenter	M <sub>W</sub>
A1	122	80	-135	285	19	36.6613°N 3.0956°W	0-15	36.6613°N 3.0956°W	6.7
A2	122	80	-135	285	19	36.6613°N 3.0956°W	0-15	36.6613°N 3.0956°W	6.9
AI1	205	80	5	1100	55	36.348°N 3.271°W	0-20	36.348°N 3.271°W	7.0
AI2	212	80	5	1520	76	36.602°N 3.052°W	0-20	36.348°N 3.271°W	7.0
AV1	290	80	-180	490	49	36.2286°N 3.3106°W	0-10	36.2286°N 3.3106°W	6.7
AV2	290	80	-180	490	49	36.2286°N 3.3106°W	0-10	36.2286°N 3.3106°W	7.0
B	134	70	-135	240	20	36.6233°N 2.7967°W	0-12	36.6233°N 2.7967°W	6.7
C1	62	90	0	228	19	36.292°N 3.059°W	0-12	36.346°N 2.980°W	6.7
C2	63	90	0	240	21	36.387°N 2.885°W	0-12	36.387°N 2.885°W	6.7
C3	53	90	0	264	22	36.4868°N 2.6869°W	0-12	36.4868°N 2.6869°W	6.7
D1	31	90	0	480	48	36.3563°N 3.4464°W	0-10	36.3563°N 3.4464°W	6.7
D2	31	90	0	480	48	36.3563°N 3.4464°W	0-10	36.3563°N 3.4464°W	7.0
LV1	121	80	35	297	27	36.7511°N 2.7089°W	0-12	36.7511°N 2.7089°W	6.7
LV2	121	80	35	297	27	36.7511°N 2.7089°W	0-12	36.751°N 2.7089°W	6.9

**Table 1** Fault parameters for the eight proposed candidate ruptures considered as possible sources for the Alborán earthquake. The fault traces are presented in Figure 3 and named as follows: A1, A2: Adra Fault ruptures; AI1 and AI2: Al-Idrissi Fault ruptures; AV1, AV2: Averroes Fault ruptures; B: Balanegra Fault rupture; C1, C2, C3: Carboneras Fault ruptures; D1 and D2: Djibouti Fault ruptures; LV1, LV2: Loma del Viento Fault ruptures. SD: seismogenic depth (upper-lower) from the QAFI database (Quaternary Active Faults of Iberia; [García-Mayordomo et al., 2012](#)).

$$R_{\text{obs-rup}} = I_{\text{obs}} - I_{\text{rup}}, \quad (1)$$

where  $I_{\text{obs}}$  is the observed intensity value, and  $I_{\text{rup}}$  is the simulated intensity value sampled from the same location as  $I_{\text{obs}}$ . The scenario that shows  $R_{\text{obs-rup}}$  closest to zero, as well as the most similar spatial pattern to  $I_{\text{obs}}$ , would be the one that best fits the observed effects of the earthquake. This means the candidate rupture upon which the best-performing scenario was built would be the closest to the actual seismic source of the earthquake. If two or more scenarios show  $R_{\text{obs-rup}}$  equally closer to zero, and both their spatial patterns fit that of  $I_{\text{obs}}$ , we proceed on to step 3 with those scenarios (“competing scenarios” henceforth).

**3. Differential zones.** We compare the competing scenarios to find the areas in which they differ from each other, or “differential zones”. If there are enough  $I_{\text{obs}}$  data points inside the differential zones, we perform a Kolmogorov–Smirnov (K–S) statistical test ([Massey, 1951](#)) to evaluate the likeness of the data distributions sampled inside these areas from  $I_{\text{obs}}$  and each

seismic scenario. The aim is to find the scenario which is statistically more similar to  $I_{\text{obs}}$ . If there are not enough data points inside the differential areas, we proceed on to step 4 with the candidate ruptures for the competing scenarios. The statistical analysis should not be performed for a differential zone if there are less than 10 points inside it.

**4. Coulomb stress transfer.** We model the static stress change ( $\Delta\text{CFS}$ ) associated with the ruptures selected as candidates using the Coulomb 3.4 software ([Toda et al., 2011](#)) and the [Okada \(1992\)](#) equations for dislocations in an elastic half-space following the methodology described by [King et al. \(1994\)](#) and [Harris \(1998\)](#). For the  $\Delta\text{CFS}$  calculations, we use a 0.4 apparent friction coefficient ([Harris, 1998](#)). We also model the source for the 25<sup>th</sup> August earthquake proposed by [de Pro-Díaz et al. \(2023\)](#), which we call rupture August. We then calculate the  $\Delta\text{CFS}$  produced along rupture August by each of the modeled candidate ruptures for the January event. We assume the 13<sup>th</sup> January earthquake might have triggered the 25<sup>th</sup> August earthquake, based

on their closeness in space and time. Under this assumption, the rupture which produces the largest area of positive  $\Delta\text{CFS}$  along rupture August will be considered as the closest to the actual source of the 13<sup>th</sup> January earthquake.

## 4 Results

### 4.1 Search for possible sources

Following the hypothesis of the offshore source, candidate faults for the 1804 Alborán earthquake have been selected among faults with Quaternary activity evidence included in the QAFI database compiled by García-Mayordomo et al. (2012) (last updated in 2022), but also from those documented by Canari et al. (2024) and Gràcia et al. (2019). Candidate faults must have been active and be located less than 40 km away from either the highest intensity points ( $I_{\text{max}}$  VII) or the epicenter proposed by Molina et al. (2018), since these authors consider the S–P arrival time in their calculations. The selected faults are the Balanegra Fault (BF), the Adra Fault (AF), the northern sector of the Al-Idrissi Fault (AIF), the Averroes Fault (AvF), the Djibouti Fault (DF), the sea extension of the Loma del Viento Fault (LVF), and three different sectors of the Carboneras Fault (CF).

For the AF, AvF, DF, BF and LVF we use the maximum mapped length for which geomorphological evidence has been reported in the bibliography. We divide the CF into segments with lengths according to the earthquake's magnitude using the empirical relations of Stirling et al. (2002) and Wells and Coppersmith (1994). For the AIF scenario, we try two possible variations: first, AI1 is a slightly larger area comprising the north and central segments; second, AI2 is an extension of the north segment linking with the North–South Faults (NSF) considering the possibility that these faults constitute a shallow sinistral shear zone related to a deeper fault that could be the northward continuation of the AIF (as proposed by Gràcia et al., 2019).

Initially, for most of the ruptures we tried the highest magnitude proposed in the bibliography,  $M_W$  6.7. However, as it will be shown later, intensities generated using this magnitude slightly underestimated  $I_{\text{obs}}$ , and some of the ruptures had areas which could generate higher  $M_W$  according to Stirling et al. (2002)'s and Wells and Coppersmith (1994)'s empirical relationships. This was the case for the AF, AvF, DF and LVF. For these ruptures, we also try these higher magnitudes. In the case of the AIF, both candidate ruptures were built initially with  $M_W$  7.0 because of their larger area and more distant location to the coast, which might have attenuated the intensity at the  $I_{\text{obs}}$  sites.

We have considered a total of fourteen different candidate ruptures, which are shown in Figure 3. Each candidate's fault parameters are presented in Table 1. Ruptures have been named using the initial letters of the rupturing fault, so rupture B for instance corresponds to the Balanegra Fault. Rupture A1 corresponds to the Adra Fault with  $M_W$  6.7, and rupture A2 corresponds to the same fault with the maximum  $M_W$  calculated for its area with the aforementioned empirical equations. The

same applies for the Loma del Viento Fault and ruptures LV1 and LV2, as well as the Djibouti Fault and ruptures D1 and D2, and the Averroes Fault and ruptures AV1 and AV2. As for the Carboneras Fault, ruptures C1, C2, and C3 correspond to three consecutive sectors of the fault with similar areas and  $M_W$  6.7.

The methodology proposed by de Pro-Díaz et al. (2022, 2023) included the use of Gasperini et al. (1999, 2010)'s method to search for candidate faults, but as stated before, this method cannot usually be applied to offshore earthquakes. For the convenience of any reader interested on this issue, we calculated the boxer for the 1804 Alborán earthquake and present the result in Figure S1 of the supplement of this work. The boxer result, as expected, does not resemble any known fault in the area, active or not, and it is located mostly onshore in disagreement with the consensus of an offshore earthquake source. This result has not been considered in the analysis and is only presented as an example of applicability limitations of the Gasperini method.

### 4.2 Seismic scenarios

Seismic scenarios built for each of the candidate ruptures presented in Table 1 are shown in Figures 4, 5 and 6. Overall, no scenario shows an optimal correspondence with  $I_{\text{obs}}$  spatial distribution. PGA-based scenarios predict higher intensities near the epicenter, while PGV-based scenarios seem to attenuate intensity less with the distance to the fault resulting in larger isoseismal areas.

Figures 7 and 8 show the residuals between observed and simulated intensity ( $R_{\text{obs-rup}}$ ) for all the scenarios using the best-performing combination of GMM–GMICE (Figure 7) and the combination that performed the poorest (Figure 8). In Figures 7 and 8, the dots represent the average of the residuals for each scenario, while the error bars represent the standard deviation. Scenarios that are more similar to  $I_{\text{obs}}$  will have  $R_{\text{obs-rup}}$  closer to 0 and narrower standard deviation bars. A scenario that is underestimating intensities will show  $R_{\text{obs-rup}} > 0$ , while a scenario that overpredicts intensities will on the other hand show  $R_{\text{obs-rup}} < 0$ . The combination of Akkar and Bommer (2010)'s GMM and Caprio et al. (2015)'s GMICE performed consistently better in terms of residuals, so all scenarios presented in this work are built on this GMM–GMICE combination. Scenarios built on any other combination systematically underestimated intensities for all candidate ruptures, so they have not been used in the rest of the analysis. For the convenience of the curious reader, we show scenarios built on the worst-performing combination, Campbell and Bozorgnia (2014)'s GMM and Worden et al. (2012)'s GMICE, in Figures S2, S3 and S4 of the supplement of this work.

Figure 7 shows the differences between the 14 scenarios and between PGA-based and PGV-based simulations. As it is shown in Figures 4, 5 and 6, PGA-based scenarios seem to slightly underestimate intensities, while PGV-based scenarios show  $R_{\text{obs-rup}}$  closer to 0 and with narrower standard deviations. A wider standard deviation is linked with a bigger discrepancy between  $I_{\text{obs}}$  spatial

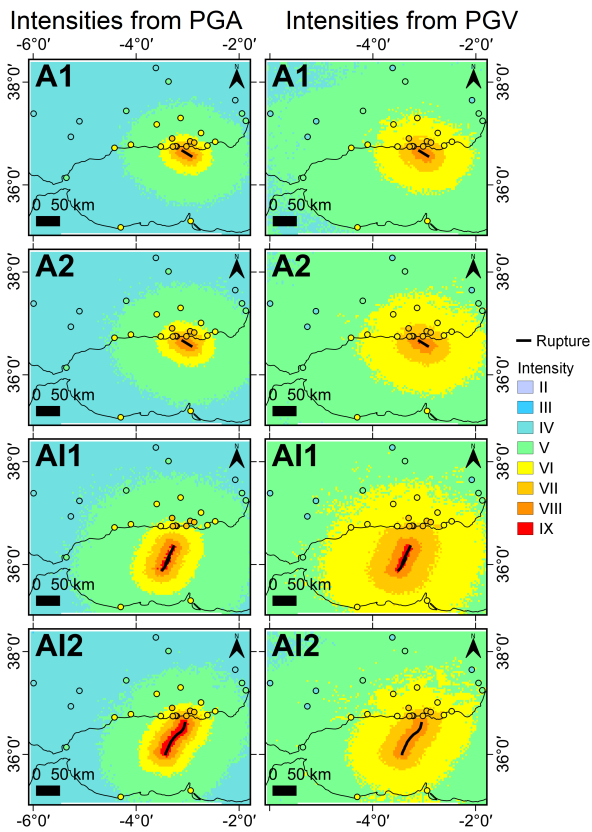


**Figure 4** Seismic scenarios built for candidate ruptures A1 and A2 (Adra Fault), and AI1 and AI2 (Al-Idrissi Fault). The dots correspond to the observed intensity recordings. Both the simulated scenario and the observed intensity data points are in the same color palette.

pattern and the scenario’s intensity spatial pattern. This can also be seen in Figures 9 and 10, which show the histograms of each scenario’s  $R_{obs-rup}$  (PGA-based scenarios in Figure 9, PGV-based scenarios in Figure 10). For instance, scenario LV1 and A1’s average  $R_{obs-rup}$  are both similarly close to 0 (Figure 7) because both scenarios predict a range of intensities that overall is close to  $I_{obs}$ . However, LV1’s simulated intensity values differ from  $I_{obs}$  values precisely on the sampling locations, and because of this, scenario LV1’s standard deviation is wider than A1’s. In other words, the range of simulated intensities for LV1 may be correct, but the values themselves are not in the correct location. The same happens with the rest of the scenarios that show discrepancies with the  $I_{obs}$  spatial pattern in Figures 4, 5 and 6.

Scenarios A1 and A2 (Figure 4) seem to have a good fit with  $I_{obs}$  spatial distribution in the epicentral area, although PGV-based scenarios show better agreement with the observed data than PGA-based ones. In both PGV-based A1 and A2 scenarios, the simulated VII isoseismal includes all  $I_{obs}$  VII points. Additionally, in PGV-based A2 scenario, most of the  $I_{obs}$  VI are also inside the simulated VI isoseismal, with the exception of the two points in the African coast and the westernmost one in the Iberian coast. In PGA-based scenarios, most  $I_{obs}$  VI points are inside the simulated V isoseismal. It is not an optimal correspondence, but PGV-based scenario A2’s performance is good enough to consider the Adra Fault

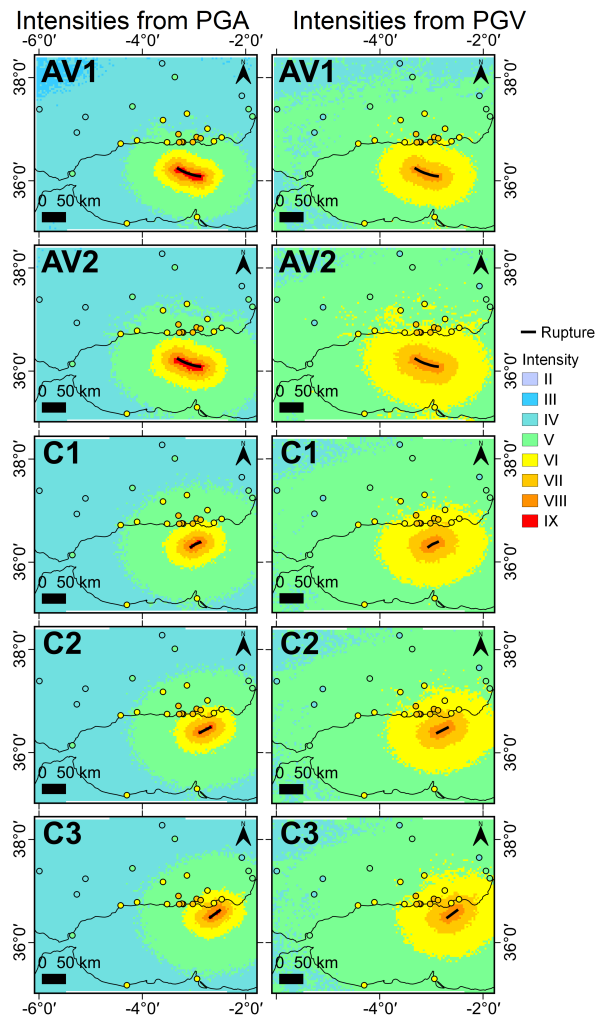


**Figure 5** Seismic scenarios built for candidate ruptures AV1 and AV2 (Averroes Fault), and C1 to C3 (Carboneras Fault). The dots correspond to the observed intensity recordings. Both the simulated scenario and the observed intensity data points are in the same color palette.

as a possible and likely source for the Alborán earthquake.

Scenarios AI1 and AI2 (Figure 4) also show an overall good fit with  $I_{obs}$  spatial distribution, except for PGA-based scenario AI1, in which almost every  $I_{obs} \geq VI$  point is in a simulated isoseismal one degree lower. Most of the  $I_{obs}$  VII points in PGV-based scenario AI1, however, are inside the simulated VII isoseismal; all of the  $I_{obs}$  VI points are inside the simulated VI isoseismal, including those in the African coast. In PGA-based scenario AI2, most of the  $I_{obs}$  VII points are inside the simulated VII isoseismal, but the majority of the  $I_{obs}$  VI points are inside the simulated V (instead of VI) isoseismal. The best performing scenario for the AIF is clearly the PGV-based AI2: almost all of the  $I_{obs}$  VII and VI are inside their corresponding simulated isoseismals. Because of this, we consider the Al-Idrissi Fault as a highly likely source for the Alborán earthquake. Between the two proposed variations, the northwards extension (AI2) seems to have the best correspondence with  $I_{obs}$  spatial distribution.

Scenarios AV1 and AV2 (Figure 5) show the clearest discrepancy among all scenarios presented here with

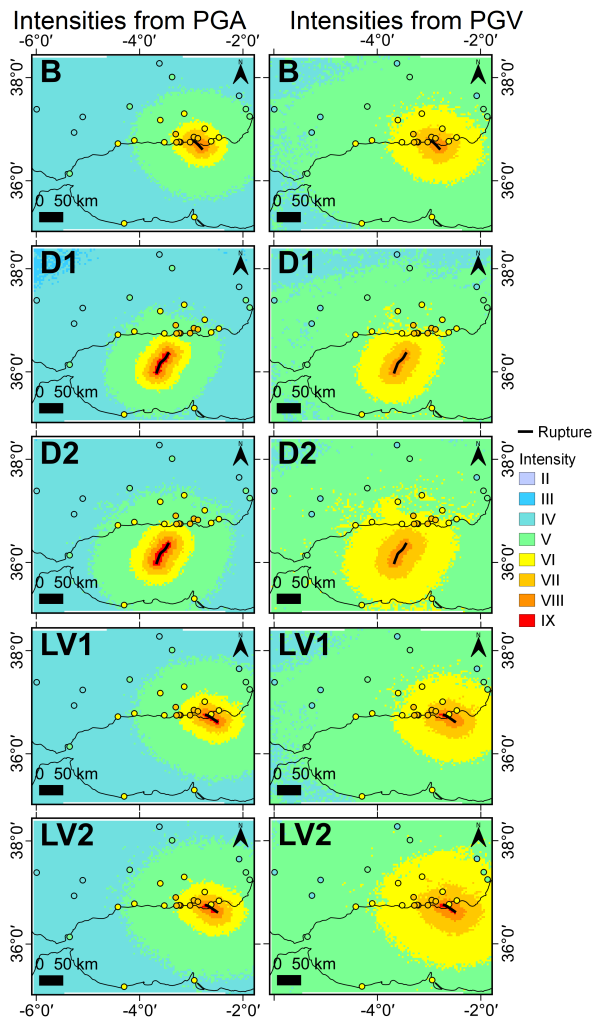


**Figure 6** Seismic scenarios built for candidate ruptures B (Balanegra Fault), D1 and D2 (Djibouti Fault), and LV1 and LV2 (Loma del Viento Fault). The dots correspond to the observed intensity recordings. Both the simulated scenario and the observed intensity data points are in the same color palette.

$I_{obs}$  spatial distribution at both the near field and the far field. The simulated VII isoseismal does not reach the Iberian coast nor any of the  $I_{obs}$  VII points in any of the cases, and the simulated VI isoseismal only reaches some of the  $I_{obs}$  VI and VII in the PGV-based scenarios. Because of these differences, we discard the Averroes Fault as a possible source for the Alborán earthquake.

Scenarios C1, C2, and C3 (Figure 5) share a similar issue with the simulated VII isoseismal not reaching (or barely reaching) the  $I_{obs}$  VII points, which are located inside the simulated VI isoseismal in the best-fitting case (PGV-based scenario C2) and inside the simulated V or even IV isoseismals in all the other cases. Moreover, the simulated VI isoseismal does not reach the African coast in any case, and for scenario C3 there are some  $I_{obs}$  VI points inside the simulated VII isoseismal. Because of all of this, we consider the Carboneras Fault as an unlikely source for the Alborán earthquake.

The simulated VIII isoseismal in scenario B (Figure 6) reaches the Iberian coast, leaving some  $I_{obs}$  VII points inside this simulated isoseismal. In the PGA-based B

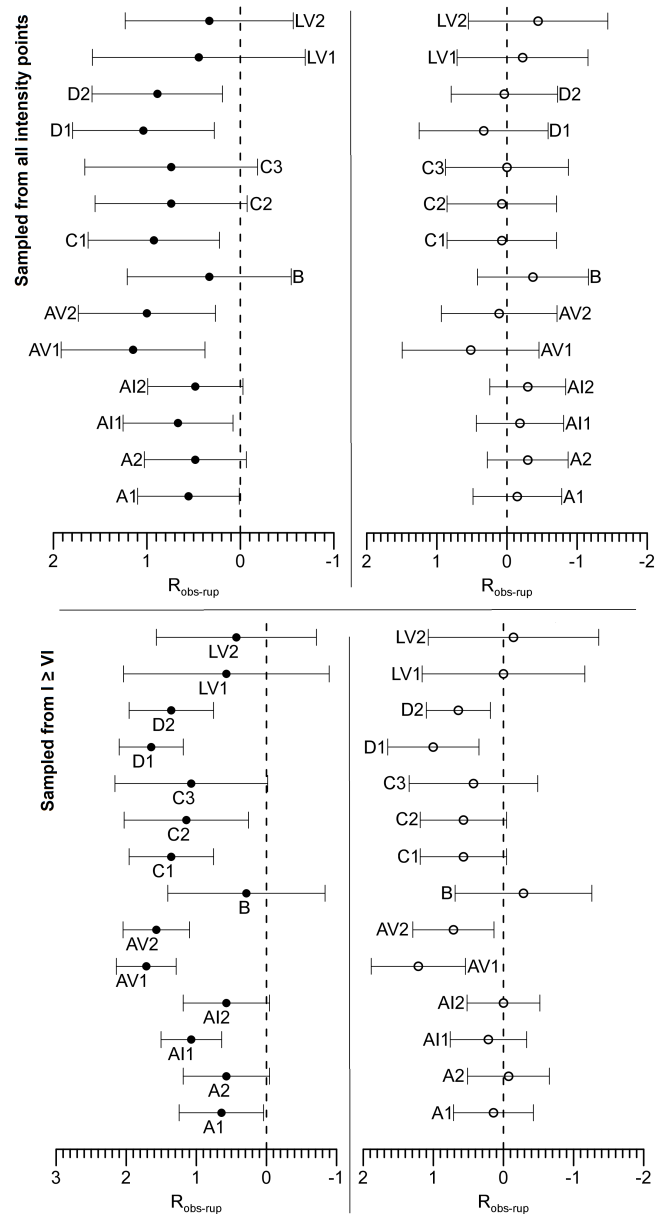


**Figure 7** Residuals  $R_{obs-rup}$  for each of the scenarios for the Alborán earthquake using the Akkar and Bommer (2010) GMM and the Caprio et al. (2015) GMICE. The average residual is represented with a dot and the bars represent the standard deviation. Black dots correspond to results from scenarios with intensities calculated from PGA, and white dots correspond to results from scenarios with intensities calculated from PGV. The graph in the top shows residuals calculated using all  $I_{obs}$  data points as sampling points. The graph in the bottom shows residuals calculated using only points with  $I_{obs} \geq VI$  as sampling points.

scenario, most of the  $I_{obs}$  VI points are in the simulated V or IV isoseismal areas, and the simulated VII isoseismal does not reach more than half of the  $I_{obs}$  VII points. This issue is less pronounced in the PGV-based B scenario, but this scenario still shows several  $I_{obs}$  VI points in the simulated V isoseismal, including those in the African coast. Because of these differences we do not consider the Balanegra Fault as a likely source for the Alborán earthquake.

The simulated VII isoseismal in scenarios D1 and D2

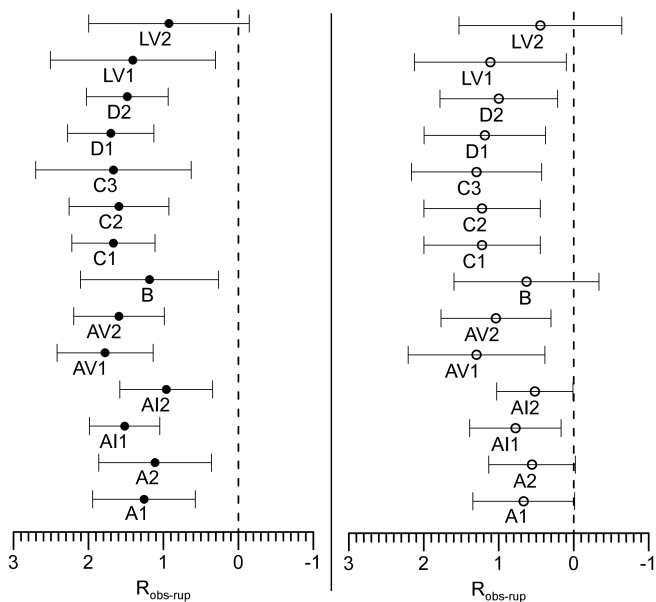


**Figure 8** Residuals  $R_{obs-rupt}$  for each of the scenarios for the Alborán earthquake using the [Campbell and Bozorgnia \(2014\)](#) GMM and the [Worden et al. \(2012\)](#) GMICE. The average residual is represented with a dot and the bars represent the standard deviation. Black dots correspond to results from scenarios with intensities calculated from PGA, and white dots correspond to results from scenarios with intensities calculated from PGV. Each scenario is labeled below the dot.

(Figure 6) does not reach the Iberian coast, so all of the  $I_{obs}$  VII points there are located inside the simulated VI isoseismal in the best-fitting case (PGV-based D2 scenario). The simulated VI isoseismal does reach the African coast and the  $I_{obs}$  VI points there. However, the difference in spatial patterns at the Iberian coast leads us to discard the Djibouti Fault as a likely source for the Alborán earthquake.

Scenarios LV1 and LV2 (Figure 6) show a clear discrepancy between  $I_{obs}$  spatial distribution and the simulated isoseismals at the epicentral area. In the PGV-based LV1 scenario, most of the  $I_{obs}$  VII points are in the simulated VI isoseismal area. There are also two  $I_{obs}$  VI points inside the simulated VII isoseismal and even one  $I_{obs}$  VI point and one  $I_{obs}$  VII inside the simulated VIII isoseismal, which reaches the Iberian coast. This spatial discrepancy is even greater in the PGA-based scenarios, with several  $I_{obs}$  VI points inside the simulated V isoseismal. The simulated VI isoseismal does not reach the African coast in any of the LV scenarios. All these differences in the intensity spatial patterns lead us to discard the Loma del Viento Fault as a possible source for the Alborán earthquake.

Considering scenarios A1, A2, AI1, and AI2 show the narrowest standard deviation and  $R_{obs-rupt}$  closest to 0, as well as the slightly better fit of A2's spatial pattern versus A1's, and AI2's versus AI1's, we moved on to the next step of the analysis with A2 and AI2 as competing scenarios.

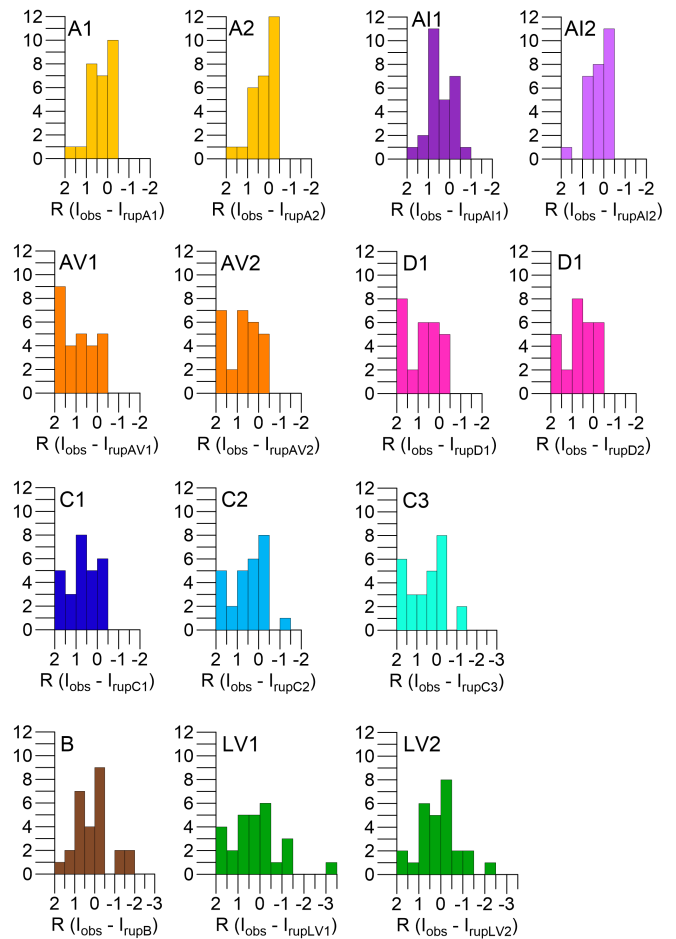


**Figure 9** Histograms for the values of the residuals  $R_{obs-rupt}$  of each PGA-based scenario.

### 4.3 Differential zones

We compare the competing scenarios selected in the previous step, A2 and AI2, by analyzing their intensity value distributions inside the differential zones: the areas in which two competing scenarios show different intensity values (Figure 11). There are several differential zones for the competing scenarios, but only two of them have  $I_{obs}$  data points inside: a smaller one north of the candidate ruptures, and a larger one southwards. There are only two  $I_{obs}$  data points inside the northern area and a single point inside the southern one, which is not enough for any statistical analysis. Because of this, the third step of the methodology proposed by [de Pro-Díaz et al. \(2023\)](#) could not be applied to the competing scenarios. This means this methodology so far does not allow us to discern the best candidate between A2 and AI2, so we moved on to the fourth and final step with these two candidates.

### 4.4 Coulomb stress transfer

In this step, we model the static stress change ( $\Delta CFS$ ) produced by ruptures A2 and AI2 on the fault plane that may have ruptured during the 25<sup>th</sup> August 1804 earthquake, which we call rupture August. This rupture involves two faults, the Loma del Viento Fault (LVF) and the Llano del Águila Fault (LLAF) ([de Pro-Díaz et al., 2023](#)). For this part of the analysis, we assume the 13<sup>th</sup>

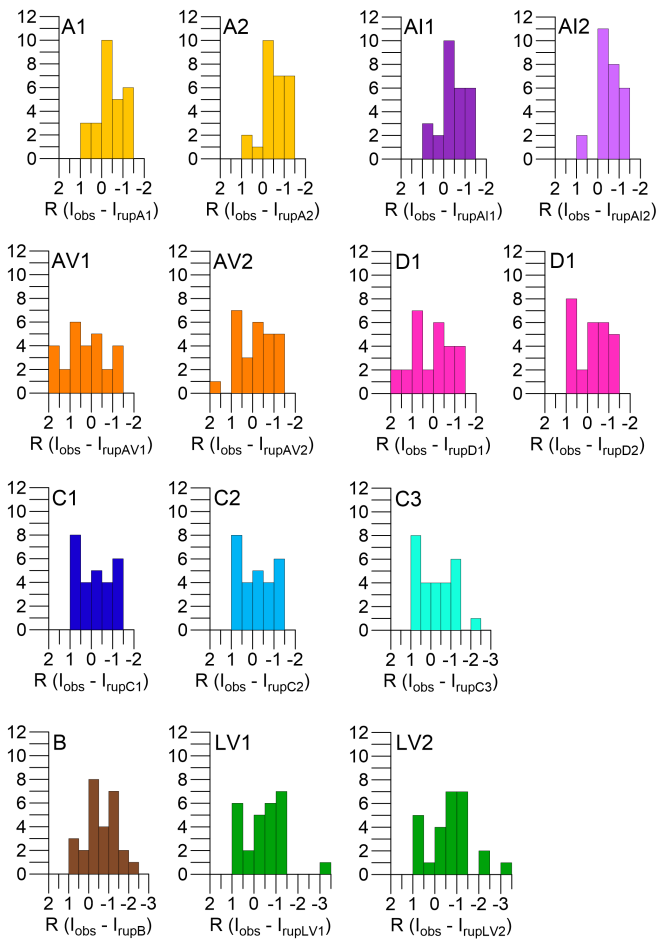


**Figure 10** Histograms for the values of the residuals  $R_{obs-rup}$  of each PGV-based scenario.

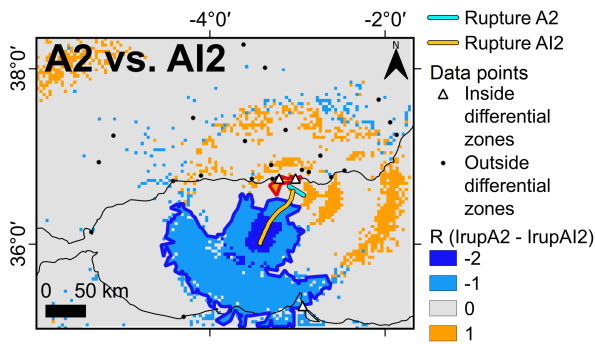


**Figure 11** Differential zones for scenarios A2 and AI2.

January and the 25<sup>th</sup> August shocks may be related by a triggering process; this assumption is supported by their closeness in time and space. If this assumption is true, the rupture which causes  $\Delta CFS > 0$  on most of rupture August’s fault plane would be the most likely source of the January shock. For each  $\Delta CFS$  calculation, we measure the area with  $\Delta CFS > 0$  on rupture August.

Rupture A2 induced  $\Delta CFS > 0$  in a 353 km<sup>2</sup> area, which is 65 % of rupture August’s surface. Maximum  $\Delta CFS$  in this case is 1.76 bar, and the average  $\Delta CFS$  in the loaded area is 0.67 bar. The stress increases on most of the LLAFF’s surface and on a wide band on the northern half of the LVF, while it decreases on the northern termination of the larger fault and on a shallow patch on its southern half (Figure 12). Rupture AI2 induced

$\Delta CFS > 0$  in a 254 km<sup>2</sup> area, which is 47 % of rupture August’s surface. Maximum  $\Delta CFS$  in this case is 1.14 bar, and the average  $\Delta CFS$  in the loaded area is 0.75 bar. The stress increases over a wide band in the southernmost sector of the LVF, and it decreases over most of the rest of the larger fault and almost the entirety of the LLAFF (Figure 13).

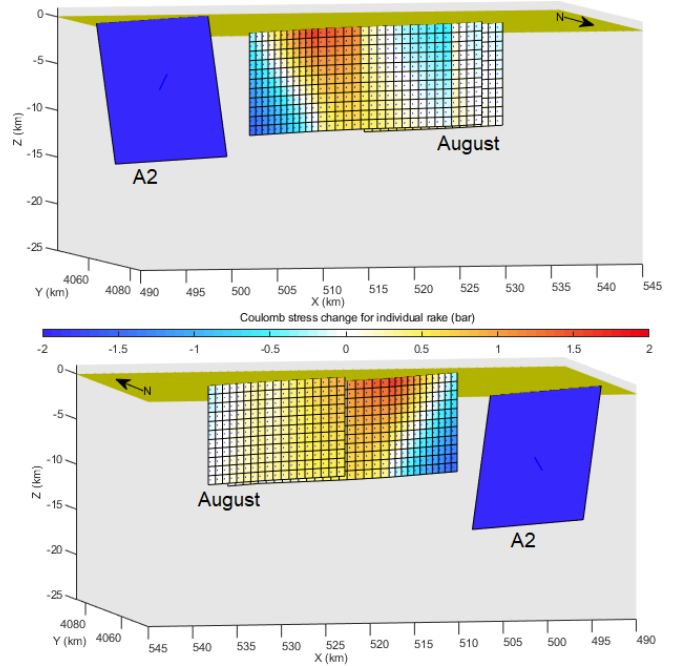


**Figure 12** Coulomb static stress change model in rupture August (Loma del Viento Fault + Llano del Águila Fault) caused by rupture A2 (Adra Fault).

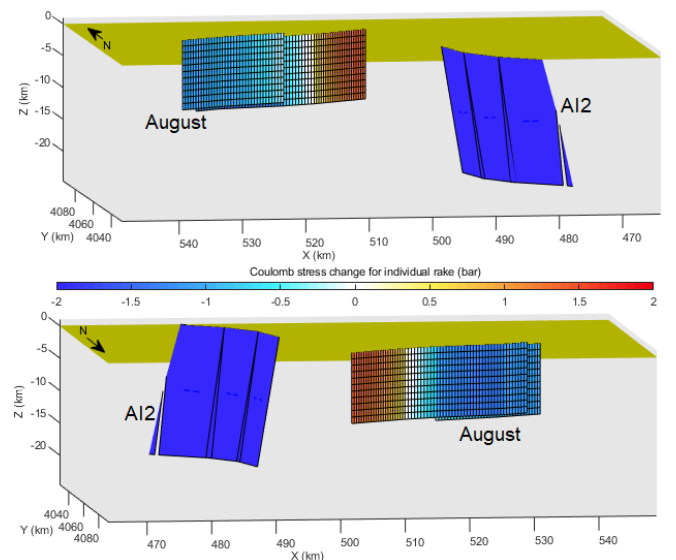


**Figure 13** Coulomb static stress change model in rupture August (Loma del Viento Fault + Llano del Águila Fault) caused by rupture AI2 (Al-Idrissi Fault + North-South Faults).

## 5 Discussion

### 5.1 Earthquake source discussion and methodology limitations

In this work, we have searched for the most likely source of the 13<sup>th</sup> January 1804 Alborán earthquake combining different methodologies. First, we searched for documented active faults that might be possible sources for the earthquake, or candidate faults (Gasperini et al., 1999, 2010). Then, we built intensity scenarios for several possible candidates to be the earthquake source and compared each of them with the observed intensity field, searching for the scenario that best agrees with the actual earthquake effects, following de Pro-Díaz et al. (2022, 2023)'s method. Finally, we used static Coulomb stress change calculations to refine the results.

None of the scenarios built for the Alborán earthquake show an optimal correlation with the intensity field's distribution when using the seismic scenario method, as seen in earlier works (de Pro-Díaz et al., 2022, 2023), but scenarios AI2 and A2 showed the best agreement with the intensity field distribution. However, the statistical tests could not be applied in the differential zones step for these two competing scenarios. This is due to the reduced amount of intensity data points inside the differential areas (less than 10), which has proven to be the main limitation of the seismic scenario methodology. A similar issue appeared while studying the 1680 Málaga earthquake (de Pro-Díaz et al., 2023), another earthquake which showed an azimuthal coverage of 180° or less on its intensity field and a high dispersion of the data points over a wide area. Poor azimuthal coverage combined with high point dispersion of the intensity field are clearly the main limitations of this methodology. These characteristics are typically present in offshore earthquakes, due to the spatial bias of intensity data; although some earthquakes of  $M_W > 7$  may cause such shaking that even if the seismic source is located offshore, there could be enough intensity points inland to apply this methodology. This was the case of the 1755 Lisbon earthquake, which was studied by Silva et al. (2023) with a methodology slightly different to the one used here but also based on building seismic scenarios and comparing them with the observed effects of the earthquake.

The implementation of the Coulomb stress transfer analysis step into the methodology is a parallel approach to strengthen the results and try to discern the best candidate rupture when the intensity data's azimuthal coverage is too poor. In this case study, assuming that there was a triggering effect between the Alborán earthquake of January 1804 and the Dalías earthquake of August 1804 considering their closeness in both space and time, our results with the Coulomb stress transfer suggest the Adra Fault would be the most likely source for the January shock. However, we must bear in mind that this triggering is an assumption, and its occurrence has not been demonstrated. We must also remember that, despite none of the scenarios tried in this work showing an optimal agreement with the in-

tensity field, the intensity spatial distribution of scenarios from the Al-Idrissi Fault extended along the North-South Faults deformation zone seem to be slightly more similar to the observed intensity distribution than the scenario from the AF is. Furthermore, Gràcia et al. (2012) already linked the AF with the 1910  $M_W > 6$  Adra earthquake. Considering the slow deformation rate in the study area, a scenario with the northern segment of AIF+NSF as the source of the 1804 Alborán earthquake might be more probable than two  $M_W > 6$  earthquakes in a 100-year span in the AF. Thus, based on our results and the antecedents of the area, we propose the combination of the Al-Idrissi Fault and the North-South Faults as the most likely source of the Alborán earthquake of 13<sup>th</sup> January 1804.

### 5.2 Influence of GMM-GMICE choice

We have tried different combinations of two GMMs and GMICES in this work. When using Campbell and Bozorgnia (2014)'s GMM and Worden et al. (2012)'s GMICE, none of the candidate ruptures generated intensities high enough to match the observed earthquake effects, not even with  $M_W$  higher than those proposed by other authors (Figure 8). We considered four possible explanations for this underestimation of the scenarios: a) the best candidate was another unknown fault we were not considering; b) the earthquake rupture might be longer than the ones we were using, which would also increase the magnitude; c) this earthquake could be a case in which complex ruptures involving several faults or fault segments lead to a higher energy release, and thus to greater damage than expected, as was observed for the Kaikoura earthquake of 2016 (e.g., Goded et al., 2017; Kaiser et al., 2017; Stirling et al., 2017; Hamling, 2019); and d) the GMM-GMICE combination was underestimating the intensities.

The aforementioned absence of evidence for this hypothetical unknown fault's existence despite intense active tectonics study in the area made option a) highly unlikely; although it cannot be completely dismissed, we do not have the resources to test it. We discarded option b) because there was no geomorphologic evidence to further extend the fault traces of the BF, AF or DF; and while the LVF could be extended inland, its intensity spatial distribution would not agree with the observed data. In addition to this, extending rupture AI1 further down the south of the AIF did not affect the predicted intensity distribution in the Iberian Peninsula, only in the African coast. As for the CF and AVF, their intensity distribution does not match the observed data and increasing the magnitude by extending the rupture would not change this. Exploring option c) would require another separate study on its own, so we did not address this option in this work. We were then down to option d): the GMM-GMICE combination being the source of the issue. Testing the GMM of Akkar and Bommer (2010) and the GMICE of Caprio et al. (2015) supported option d): the predicted intensities increased significantly in all of the scenarios, with some of them showing a rather good agreement (although not optimal) with the observed intensity distribution. An example of this is

shown in Figure 14 with the AI2 scenario. The Campbell and Bozorgnia (2014) and Worden et al. (2012) combination was recommended by de Pro-Díaz et al. (2023) using the Lorca earthquake of 2011 as a calibration event, but this was a  $M_W$  5.2 earthquake generated by an inland fault and much smaller than the Alborán earthquake. Because of these differences between the two events, the initial GMM–GMICE combination was most likely not adequate for a  $M_W > 6$  earthquake. This testing highlights the importance of choosing a GMM–GMICE combination that is representative of the study area. A revision of the scenarios presented in de Pro-Díaz et al. (2023) with the Akkar and Bommer (2010) GMM and the Caprio et al. (2015) GMICE might be interesting for future works.

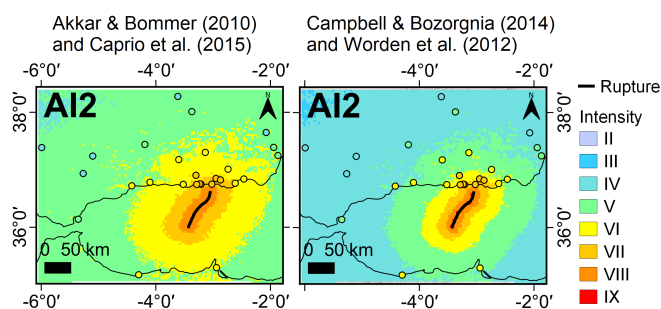


**Figure 14** Comparison of the AI2 scenario built on two different combinations of GMM and GMICE. The observed intensity field is superimposed in the same color palette.

### 5.3 Reported vs. modelled $M_W$

Even with the best performing GMM–GMICE combination, most scenarios using a  $M_W$  equal to the maximum value calculated by other authors seem to underestimate the intensity values at some of the  $I_{obs}$  data sites, especially the  $I_{obs}$  VI points farther from the epicentral area. Martínez Solares and Mezcua Rodríguez (2002), Posadas et al. (2006) and Mezcua et al. (2013) estimated this earthquake’s magnitude using Bakun and Wentworth (1997)’s method, which uses macroseismic data from a large number of earthquakes in the same area to calculate an equation that relates the maximum observed intensity at the macroseismic epicenter with magnitude. This method, just like Gasperini et al. (1999, 2010), requires a good azimuthal coverage of the intensity observations around the epicenter of the earthquake of interest; otherwise, the macroseismic epicenter might be mislocated, and the observed intensity used to calculate the magnitude would not be the maximum intensity, thus leading to underestimating the magnitude. The unreliability of this kind of calculation when intensity data are scarce and so heterogeneously distributed over the study area, as in this case, has been shown before in this study and in previous work (de Pro-Díaz et al., 2023). It is therefore possible that Martínez Solares and Mezcua Rodríguez (2002), Posadas et al. (2006) and Mezcua et al. (2013) underestimated this earthquake’s magnitude. In addition to this, according to the equations of Stirling et al. (2002) and Wells and Coppersmith (1994),  $M_W > 6.7$  is plausible

for the considered rupture areas in the best performing scenarios in this work. In the case of the AIF, Gràcia et al. (2019) noted this fault’s potential to generate  $M_W \geq 7$  earthquakes. We may never know with precision whether the actual  $M_W$  was 7.0, 6.9, or a lower number, considering this is a pre-instrumental earthquake. However, our results show that  $M_W < 6.9$  might not explain the observed damage distribution, but higher magnitudes in any of the nearby faults would. This possibility should be considered in future seismic hazards assessments in this area. The proposed methodology could also be applied to better state uncertainties in  $M_W$  calculations for offshore historical earthquakes.

## 6 Conclusions

We have applied the seismic scenario method and Coulomb stress transfer analysis to investigate the most likely source of the 1804 Alborán earthquake. The seismic scenario method allowed us to discard 12 out of 14 possible candidate ruptures, but the observed intensity field was too scarce and lacked the azimuthal coverage needed to discern the best candidate among the remaining two (the Adra Fault with  $M_W$  6.9, and the Al-Idrissi plus North–South Faults with  $M_W$  7.0). The results of the Coulomb stress transfer analysis allowed us to rank these two candidates, but only with the assumption of an unproven triggering effect between the Alborán shock of 13<sup>th</sup> January and the Dalías shock of 25<sup>th</sup> August. In the end, considering our results and the seismicity antecedents of the area, we propose the combination of the northern Al-Idrissi Fault segment with the North–South Faults as the most likely source for the 1804 Alborán earthquake. The Alborán earthquake might have had a higher magnitude than the values proposed by other authors ( $M_W$  6.9–7.0 compared to  $M_W$  6.3–6.7), although more research is needed into this issue.

The proposed methodology has proven to be useful when working with offshore earthquakes. This methodology may allow researchers to link historical earthquakes with their most likely responsible faults, even in remote and inaccessible areas such as marine environments. In order to work with this methodology, it is crucial to use a GMM–GMICE combination that is representative of the study area. Azimuthal coverage and density of the intensity data are the main limitations of the methodology.

## Acknowledgements

This work has been funded thanks to a predoctoral research contract from the Universidad Complutense de Madrid (2019) and its following Postdoctoral Orientation Period (POP), as well as the research project “Análisis del ciclo sísmico a largo plazo a partir de datos geológicos y modelado” with reference number PID2021-124155NB-C31. We kindly thank the reviewers who contributed with their constructive critics to help us improve this work.

## 7 Data and code availability

Data used in this work was not compiled by the authors. The authors used data from [Murphy Corella \(2019\)](#), which is an open-access book available in the digital archive of the Instituto Geográfico Nacional (<https://www.ign.es/web/libros-digitales/terremotos-almeria-1804>), and [Martínez Solares and Mezcua Rodríguez \(2002\)](#), also available in the same archive (<http://www.ign.es/web/recursos/docs/IGNCnig/SIS-Catalogo-hasta-1900.pdf>).

## 8 Competing interests

The authors have no competing interests.

## References

- Abrahamson, N., Silva, W., and Kamai, R. Update of the AS08 Ground-Motion Prediction equations based on the NGA-west2 data set. *Pacific Engineering Research Center Report*, May, 174, 2014. <http://scholar.google.com/scholar?hl=en&btnG=Search&q=intitle:Update+of+the+AS08+Ground-Motion+Prediction+Equations+Based+on+the+NGA-West2+Data+Set#0>.
- Akkar, S. and Bommer, J. J. Empirical Equations for the Prediction of PGA, PGV, and Spectral Accelerations in Europe, the Mediterranean Region, and the Middle East. *Seismological Research Letters*, 81(2):195–206, March 2010. doi: 10.1785/gssrl.81.2.195.
- Akkar, S., Sandikkaya, M. A., and Bommer, J. J. Empirical ground-motion models for point- and extended-source crustal earthquake scenarios in Europe and the Middle East. *Bulletin of Earthquake Engineering*, 12(1):359–387, May 2013. doi: 10.1007/s10518-013-9461-4.
- Allen, T. I. and Wald, D. J. *Topographic Slope as a Proxy for Seismic Site-Conditions (VS30) and Amplification Around the Globe*. 2007. doi: 10.3133/ofr20071357.
- Álvarez-Gómez, J. A., Martín, R., Pérez-López, R., Stich, D., Cantavella, J., Martínez-Díaz, J., Morales Soto, J., Martínez-García, P., Soto, J., and Carreño, E. La serie sísmica de Alhucemas 2016. Partición de la deformación e interacción de estructuras en un límite de placas difuso. *Geo-Temas*, 16(2):491–494, 2016.
- Álvarez-Gómez, J. A., Herrero-Barbero, P., and Martínez-Díaz, J. J. Seismogenic potential and tsunami threat of the strike-slip Carboneras fault in the western Mediterranean from physics-based earthquake simulations. *Natural Hazards and Earth System Sciences*, 23(6):2031–2052, June 2023. doi: 10.5194/nhess-23-2031-2023.
- Ambraseys and Jackson. Faulting associated with historical and recent earthquakes in the Eastern Mediterranean region. *Geophysical Journal International*, 133(2):390–406, May 1998. doi: 10.1046/j.1365-246x.1998.00508.x.
- Ambraseys, N. N., Douglas, J., Sarma, S. K., and Smit, P. M. Equations for the Estimation of Strong Ground Motions from Shallow Crustal Earthquakes Using Data from Europe and the Middle East: Horizontal Peak Ground Acceleration and Spectral Acceleration. *Bulletin of Earthquake Engineering*, 3(1):1–53, January 2005. doi: 10.1007/s10518-005-0183-0.
- Ammar, A., Mauffret, A., Gorini, C., and Jabour, H. The Tectonic Structure Of The Alboran Margin Of Morocco. *Revista de La Sociedad Geológica de España*, 20(3–4):247–271, 2007.
- Atkinson, G. M. and Kaka, S. I. Relationships between Felt Intensity and Instrumental Ground Motion in the Central United States and California. *Bulletin of the Seismological Society of America*, 97(2):497–510, April 2007. doi: 10.1785/0120060154.
- Atkinson, G. M. and Wald, D. J. “Did You Feel It?” Intensity Data: A Surprisingly Good Measure of Earthquake Ground Motion. *Seismological Research Letters*, 78(3):362–368, May 2007. doi: 10.1785/gssrl.78.3.362.
- Bakun, W. H. and Wentworth, C. M. Estimating earthquake location and magnitude from seismic intensity data. *Bulletin of the Seismological Society of America*, 87(6):1502–1521, 1997. doi: 10.1785/BSSA0870061502.
- Basili, R., Valensise, G., Vannoli, P., Burrato, P., Fracassi, U., Mariano, S., Tiberti, M. M., and Boschi, E. The Database of Individual Seismogenic Sources (DISS), version 3: Summarizing 20 years of research on Italy’s earthquake geology. *Tectonophysics*, 453(1–4):20–43, June 2008. doi: 10.1016/j.tecto.2007.04.014.
- Bozorgnia, Y., Abrahamson, N. A., Atik, L. A., Ancheta, T. D., Atkinson, G. M., Baker, J. W., Baltay, A., Boore, D. M., Campbell, K. W., Chiou, B. S.-J., Darragh, R., Day, S., Donahue, J., Graves, R. W., Gregor, N., Hanks, T., Idriss, I. M., Kamai, R., Kishida, T., Kottke, A., Mahin, S. A., Rezaeian, S., Rowshandel, B., Seyhan, E., Shahi, S., Shantz, T., Silva, W., Spudich, P., Stewart, J. P., Watson-Lamprey, J., Wooddell, K., and Youngs, R. NGA-West2 Research Project. *Earthquake Spectra*, 30(3):973–987, August 2014. doi: 10.1193/072113eqs209m.
- Campbell, K. W. Prediction of Strong Ground Motion Using the Hybrid Empirical Method and Its Use in the Development of Ground-Motion (Attenuation) Relations in Eastern North America. *Bulletin of the Seismological Society of America*, 93(3):1012–1033, June 2003. doi: 10.1785/0120020002.
- Campbell, K. W. and Bozorgnia, Y. NGA-West2 Ground Motion Model for the Average Horizontal Components of PGA, PGV, and 5 *Earthquake Spectra*, 30(3):1087–1115, August 2014. doi: 10.1193/062913eqs175m.
- Canari, A., Perea, H., and Martínez-Loriente, S. Characterizing an Incipient Transensional Fault System: Insights from the Morphometric Analysis of the North-South Faults (Alboran Sea). November 2024. doi: 10.22541/essoar.173153134.46086157/v1.
- Canora, C., Martínez-Díaz, J. J., Villamor, P., Berryman, K., Alvarez-Gomez, J. A., Pullinger, C., and Capote, R. Geological and Seismological Analysis of the 13 February 2001 Mw 6.6 El Salvador Earthquake: Evidence for Surface Rupture and Implications for Seismic Hazard. *Bulletin of the Seismological Society of America*, 100(6):2873–2890, December 2010. doi: 10.1785/0120090377.
- Canora, C., Vilanova, S. P., De Pro-Díaz, Y., Pina, P., and Heleno, S. Evidence of Surface Rupture Associated With Historical Earthquakes in the Lower Tagus Valley, Portugal. Implications for Seismic Hazard in the Greater Lisbon Area. *Frontiers in Earth Science*, 9, March 2021. doi: 10.3389/feart.2021.620778.
- Caprio, M., Tarigan, B., Worden, C. B., Wiemer, S., and Wald, D. J. Ground Motion to Intensity Conversion Equations (GMICEs): A Global Relationship and Evaluation of Regional Dependency. *Bulletin of the Seismological Society of America*, 105(3):1476–1490, May 2015. doi: 10.1785/0120140286.
- Caputo, R., Sboras, S., Pavlides, S., and Chatzipetros, A. Comparison between single-event effects and cumulative effects for the purpose of seismic hazard assessment. A review from Greece. *Earth-Science Reviews*, 148:94–120, September 2015. doi: 10.1016/j.earscirev.2015.05.004.
- d’Acremont, E., Gutscher, M.-A., Rabaute, A., Mercier de Lépinay, B., Lafosse, M., Poort, J., Ammar, A., Tahayt, A., Le Roy, P., Smit, J., Do Couto, D., Cancouët, R., Prunier, C., Ercilla, G., and Gorini, C. High-resolution imagery of active faulting offshore Al Hoceima, Northern Morocco. *Tectonophysics*, 632:160–166, September 2014. doi: 10.1016/j.tecto.2014.06.008.

- De Larouzière, F., Bolze, J., Bordet, P., Hernandez, J., Montecat, C., and Ott d'Estevou, P. The Betic segment of the lithospheric Trans-Alboran shear zone during the Late Miocene. *Tectonophysics*, 152(1–2):41–52, September 1988. doi: 10.1016/0040-1951(88)90028-5.
- de Pro-Díaz, Y., Vilanova, S., and Canora, C. Ranking Earthquake Sources Using Spatial Residuals of Seismic Scenarios: Methodology Application to the 1909 Benavente Earthquake. *Bulletin of the Seismological Society of America*, 113(2):710–731, December 2022. doi: 10.1785/0120220067.
- de Pro-Díaz, Y., Perea, H., Insua-Arévalo, J. M., Martínez-Díaz, J. J., and Canora, C. Constraining earthquake fault sources through the use of intensity data and seismic scenarios: application to the Betic Cordillera (South Spain). *Frontiers in Earth Science*, 11, August 2023. doi: 10.3389/feart.2023.1214836.
- Delavaud, E., Scherbaum, F., Kuehn, N., and Riggelsen, C. Information-Theoretic Selection of Ground-Motion Prediction Equations for Seismic Hazard Analysis: An Applicability Study Using Californian Data. *Bulletin of the Seismological Society of America*, 99(6):3248–3263, November 2009. doi: 10.1785/0120090055.
- DeMets, C., Gordon, R. G., and Argus, D. F. Geologically current plate motions. *Geophysical Journal International*, 181(1):1–80, April 2010. doi: 10.1111/j.1365-246x.2009.04491.x.
- Echeverría, A., Khazaradze, G., Asensio, E., and Masana, E. Geodetic evidence for continuing tectonic activity of the Carboneras fault (SE Spain). *Tectonophysics*, 663:302–309, November 2015. doi: 10.1016/j.tecto.2015.08.009.
- Espinar Moreno, M. Los estudios de sismicidad histórica en Andalucía: los terremotos históricos de la provincia de Almería. In *El estudio de los terremotos en Almería*, page 115–180. 1994. <https://dialnet.unirioja.es/servlet/articulo?codigo=2767758>. Instituto de Estudios Almerienses.
- Estrada, F., Galindo-Zaldívar, J., Vázquez, J. T., Ercilla, G., D'Acremont, E., Alonso, B., and Gorini, C. Tectonic indentation in the central Alboran Sea (westernmost Mediterranean). *Terra Nova*, 30(1):24–33, November 2017. doi: 10.1111/ter.12304.
- Ferrater, M., Ortuño, M., Masana, E., Pallàs, R., Perea, H., Baize, S., García-Meléndez, E., Martínez-Díaz, J. J., Echeverría, A., Rockwell, T. K., Sharp, W. D., Medialdea, A., and Rhodes, E. J. Refining seismic parameters in low seismicity areas by 3D trenching: The Alhama de Murcia fault, SE Iberia. *Tectonophysics*, 680:122–128, June 2016. doi: 10.1016/j.tecto.2016.05.020.
- Ferrater, M., Ortuño, M., Masana, E., Martínez-Díaz, J. J., Pallàs, R., Perea, H., Baize, S., García-Meléndez, E., Echeverría, A., Rockwell, T., Sharp, W. D., and Arrowsmith, R. Lateral slip rate of Alhama de Murcia fault (SE Iberian Peninsula) based on a morphotectonic analysis: Comparison with paleoseismological data. *Quaternary International*, 451:87–100, September 2017. doi: 10.1016/j.quaint.2017.02.018.
- Fracassi, U. and Valensise, G. Unveiling the Sources of the Catastrophic 1456 Multiple Earthquake: Hints to an Unexplored Tectonic Mechanism in Southern Italy. *Bulletin of the Seismological Society of America*, 97(3):725–748, June 2007. doi: 10.1785/0120050250.
- García-Mayordomo, J., Insua-Arévalo, J., Martínez-Díaz, J., Jiménez-Díaz, A., Martín-Banda, R., Martín-Alfageme, S., Álvarez Gómez, J., Rodríguez-Peces, M., Pérez-López, R., Rodríguez-Pascua, M., Masana, E., Perea, H., Martín-González, F., Giner-Robles, J., Nemser, E., Cabral, J., and The QAFI Compilers Working Group. The Quaternary Active Faults Database of Iberia (QAFI v.2.0). *Journal of Iberian Geology*, 38(1), September 2012. doi: 10.5209/rev\_jige.2012.v38.n1.39219.
- Gasparini, P., Bernardini, F., Valensise, G., and Boschi, E. Defining seismogenic sources from historical earthquake felt reports. *Bulletin of the Seismological Society of America*, 89(1):94–110, February 1999. doi: 10.1785/bssa0890010094.
- Gasparini, P., Vannucci, G., Tripone, D., and Boschi, E. The Location and Sizing of Historical Earthquakes Using the Attenuation of Macroseismic Intensity with Distance. *Bulletin of the Seismological Society of America*, 100(5A):2035–2066, September 2010. doi: 10.1785/0120090330.
- Goded, T., Horspool, N., Canessa, S., and Gerstenberger, M. Modified Mercalli intensities for the M7.8 Kaikōura (New Zealand) 14 November 2016 earthquake derived from 'felt detailed' and 'felt rapid' online questionnaires. *Bulletin of the New Zealand Society for Earthquake Engineering*, 50(2):352–362, June 2017. doi: 10.5459/bnzsee.50.2.352-362.
- Griffin, J., Nguyen, N., Cummins, P., and Cipta, A. Historical Earthquakes of the Eastern Sunda Arc: Source Mechanisms and Intensity-Based Testing of Indonesia's National Seismic Hazard Assessment. *Bulletin of the Seismological Society of America*, 109(1):43–65, December 2018. doi: 10.1785/0120180085.
- Gràcia, E., Pallàs, R., Soto, J., Comas, M., Moreno, X., Masana, E., Santanach, P., Diez, S., García, M., Dañoibeitia, J., Bartolomé, R., Farrán, M., Gómez, M., Alpiste, M., Lastras, G., Wilmott, V., Perea, H., Blondel, P., Gómez, O., and Roque, C. Active faulting offshore SE Spain (Alboran Sea): Implications for earthquake hazard assessment in the Southern Iberian Margin. *Earth and Planetary Science Letters*, 241(3–4):734–749, January 2006. doi: 10.1016/j.epsl.2005.11.009.
- Gràcia, E., Bartolomé, R., Lo Iacono, C., Moreno, X., Stich, D., Martínez-Díaz, J. J., Bozzano, G., Martínez-Lorient, S., Perea, H., Diez, S., Masana, E., Dañoibeitia, J. J., Tello, O., Sanz, J. L., and Carreño, E. Acoustic and seismic imaging of the Adra Fault (NE Alboran Sea): in search of the source of the 1910 Adra earthquake. *Natural Hazards and Earth System Sciences*, 12(11):3255–3267, November 2012. doi: 10.5194/nhess-12-3255-2012.
- Gràcia, E., Grevemeyer, I., Bartolomé, R., Perea, H., Martínez-Lorient, S., Gómez de la Peña, L., Villaseñor, A., Klinger, Y., Lo Iacono, C., Diez, S., Calahorrano, A., Camafort, M., Costa, S., d'Acremont, E., Rabaute, A., and Ranero, C. R. Earthquake crisis unveils the growth of an incipient continental fault system. *Nature Communications*, 10(1), September 2019. doi: 10.1038/s41467-019-11064-5.
- Grünthal, G. European Macroseismic Scale 1998, 1998. <http://lib.riskreductionafrica.org/bitstream/handle/123456789/1193/1281.European>. European Seismological Commission (ESC).
- Gómez de la Peña, L., Gràcia, E., Maesano, F. E., Basili, R., Kopp, H., Sánchez-Serra, C., Scala, A., Romano, F., Volpe, M., Piatanesi, A., and R. Ranero, C. A first appraisal of the seismogenic and tsunamigenic potential of the largest fault systems in the westernmost Mediterranean. *Marine Geology*, 445:106749, March 2022. doi: 10.1016/j.margeo.2022.106749.
- Gómez-Novell, O., García-Mayordomo, J., Ortuño, M., Masana, E., and Chartier, T. Fault System-Based Probabilistic Seismic Hazard Assessment of a Moderate Seismicity Region: The Eastern Betics Shear Zone (SE Spain). *Frontiers in Earth Science*, 8, December 2020. doi: 10.3389/feart.2020.579398.
- Hamling, I. J. A review of the 2016 Kaikōura earthquake: insights from the first 3 years. *Journal of the Royal Society of New Zealand*, 50(2):226–244, December 2019. doi: 10.1080/03036758.2019.1701048.
- Harris, R. A. Introduction to Special Section: Stress Triggers, Stress Shadows, and Implications for Seismic Hazard. *Journal of Geophysical Research: Solid Earth*, 103(B10):24347–24358, October 1998. doi: 10.1029/98jb01576.

- Herrero Barbero, P. *Modelización 3D de la estructura, la cinemática y el comportamiento sismogénico del sistema de fallas de las Béticas Orientales. Aplicación a la amenaza sísmica*. Universidad Complutense de Madrid, 2021.
- Herrero-Barbero, P., Álvarez-Gómez, J. A., Williams, C., Villamor, P., Insua-Arévalo, J. M., Alonso-Henar, J., and Martínez-Díaz, J. J. Physics-Based Earthquake Simulations in Slow-Moving Faults: A Case Study From the Eastern Betic Shear Zone (SE Iberian Peninsula). *Journal of Geophysical Research: Solid Earth*, 126(5), May 2021. doi: 10.1029/2020jb021133.
- Hough, S. E. and Graves, R. W. The 1933 Long Beach Earthquake (California, USA): Ground Motions and Rupture Scenario. *Scientific Reports*, 10(1), June 2020. doi: 10.1038/s41598-020-66299-w.
- Huerta, P., Silva, P., Giner-Robles, J., Rodríguez-Pascua, M., and Bautista Davila, M. Efectos geológicos del terremoto de Dalías-Berja 1804 AD. *Almería, SE España*. XIV Reunión Nacional de Cuaternario, 1:194–197, 2015.
- ICN-UGM. Actualización de mapas de peligrosidad sísmica de España 2012, 2013. doi: 10.7419/162.05.2017. Centro Nacional de Información Geográfica (CNIG).
- Insua-Arevalo, J. M., García-Mayordomo, J., Salazar, A. E., Rodríguez-Escudero, E., Martín-Banda, R., Álvarez-Gómez, J. A., Canora, C., and Martínez-Díaz, J. J. Paleoseismological evidence of holocene activity of the Los Tollos Fault (Murcia, SE Spain): A lately formed quaternary tectonic feature of the eastern betic shear zone. *Journal of Iberian Geology*, 41(3), February 2015. doi: 10.5209/rev\_JIGE.2015.v41.n3.49948.
- Kaiser, A., Balfour, N., Fry, B., Holden, C., Litchfield, N., Gerstenberger, M., D'Anastasio, E., Horspool, N., McVerry, G., Ristau, J., Bannister, S., Christophersen, A., Clark, K., Power, W., Rhoades, D., Massey, C., Hamling, I., Wallace, L., Mountjoy, J., Kaneko, Y., Benites, R., Van Houtte, C., Dellow, S., Wotherpoon, L., Elwood, K., and Gledhill, K. The 2016 Kaikōura, New Zealand, Earthquake: Preliminary Seismological Report. *Seismological Research Letters*, 88(3):727–739, April 2017. doi: 10.1785/0220170018.
- Kaka, S. and Atkinson, G. Relationships between Instrumental Ground-Motion Parameters and Modified Mercalli Intensity in Eastern North America. *Bulletin of the Seismological Society of America*, 94(5):1728–1736, October 2004. doi: 10.1785/0120032228.
- King, G., Stein, R., and Lin, J. Static stress changes and the triggering of earthquakes. *Bulletin of the Seismological Society of America*, 84(3):935–953, 1994. doi: 10.1785/BSSA0840030935.
- Lafosse, M., d'Acremont, E., Rabaute, A., Estrada, F., Jollivet-Castelot, M., Vazquez, J. T., Galindo-Zaldívar, J., Ercilla, G., Alonso, B., Smit, J., Ammar, A., and Gorini, C. Plio-Quaternary tectonic evolution of the southern margin of the Alboran Basin (Western Mediterranean). *Solid Earth*, 11(2):741–765, April 2020. doi: 10.5194/se-11-741-2020.
- Lozano, L., Buforn, E., Vicente Cantavella, J., López-Sánchez, C., Victoria Manzanedo, M., Barco, J., Antón, R., Cabieces, R., and Mattesini, M. Relocation of Recent Shallow Seismic Activity in the Alboran Sea (Western Mediterranean Sea): The 2021–2024, 2016, and 2004 Seismic Series. *Bulletin of the Seismological Society of America*, 115(2):469–488, January 2025. doi: 10.1785/0120240159.
- Lozos, J. C. A case for historic joint rupture of the San Andreas and San Jacinto faults. *Science Advances*, 2(3), March 2016. doi: 10.1126/sciadv.1500621.
- Marín-Lechado, C., Galindo-Zaldívar, J., Rodríguez-Fernández, L. R., Serrano, I., and Pedrera, A. Active faults, seismicity and stresses in an internal boundary of a tectonic arc (Campo de Dalías and Níjar, southeastern Betic Cordilleras, Spain). *Tectonophysics*, 396(1–2):81–96, February 2005. doi: 10.1016/j.tecto.2004.11.001.
- Marín-Lechado, C., Galindo-Zaldívar, J., Gil, A. J., Borque, M. J., De Lacy, M. C., Pedrera, A., López-Garrido, A. C., Alfaro, P., García-Tortosa, F., Ramos, M. I., Rodríguez-Caderot, G., Rodríguez-Fernández, J., Ruiz-Constán, A., and De Galdeano-Equiza, C. S. Levelling Profiles and a GPS Network to Monitor the Active Folding and Faulting Deformation in the Campo de Dalías (Betic Cordillera, Southeastern Spain). *Sensors*, 10(4):3504–3518, April 2010. doi: 10.3390/s100403504.
- Martínez-Díaz, J. *Neotectónica y Tectónica Activa del Sector Centro-Occidental de la Región de Murcia y Sur de Almería (Cordillera Bética - España)*. Universidad Complutense de Madrid, 1999.
- Martínez-Díaz, J., Masana, E., and Ortuño, M. Active tectonics of the Alhama de Murcia fault, Betic Cordillera, Spain. *Journal of Iberian Geology*, 38(1), September 2012. doi: 10.5209/rev\_jige.2012.v38.n1.39218.
- Martínez-Díaz, J. J. and Hernández-Enrile, J. L. Neotectonics and morphotectonics of the southern Almería region (Betic Cordillera-Spain) kinematic implications. *International Journal of Earth Sciences*, 93(2):189–206, April 2004. doi: 10.1007/s00531-003-0379-y.
- Martínez-García, P., Soto, J. I., and Comas, M. Recent structures in the Alboran Ridge and Yusuf fault zones based on swath bathymetry and sub-bottom profiling: evidence of active tectonics. *Geo-Marine Letters*, 31(1):19–36, June 2011. doi: 10.1007/s00367-010-0212-0.
- Martínez-Martínez, J. M. Lateral interaction between metamorphic core complexes and less-extended, tilt-block domains: the Alpujarras strike-slip transfer fault zone (Betics, SE Spain). *Journal of Structural Geology*, 28(4):602–620, April 2006. doi: 10.1016/j.jsg.2006.01.012.
- Martínez Solares, J. and Mezcua Rodríguez, J. Catálogo sísmico de la Península Ibérica (880 a. C., 2002).
- Martínez-García, P., Comas, M., Soto, J. I., Lonergan, L., and Watts, A. B. Strike-slip tectonics and basin inversion in the Western Mediterranean: The Post-Messinian evolution of the Alboran Sea. *Basin Research*, 25(4):361–387, March 2013. doi: 10.1111/bre.12005.
- Martín-Banda, R., García-Mayordomo, J., Insua-Arévalo, J. M., Salazar, Á. E., Rodríguez-Escudero, E., Álvarez-Gómez, J. A., Medialdea, A., and Herrero, M. J. New insights on the seismogenic potential of the Eastern Betic Shear Zone (SE Iberia): Quaternary activity and paleoseismicity of the SW segment of the Carrascoy Fault Zone. *Tectonics*, 35(1):55–75, January 2016. doi: 10.1002/2015tc003997.
- Massey, F. J. The Kolmogorov-Smirnov Test for Goodness of Fit. *Journal of the American Statistical Association*, 46(253):68–78, March 1951. doi: 10.1080/01621459.1951.10500769.
- McCalpin, J. P. and Nelson, A. R. Introduction to Paleoseismology. In McCalpin, J. P., editor, *Paleoseismology*, volume 62 of *International Geophysics Series*, pages 1–20. Academic Press, San Diego, CA, 1996.
- Mezcua, J., Rueda, J., and García Blanco, R. M. Iberian Peninsula Historical Seismicity Revisited: An Intensity Data Bank. *Seismological Research Letters*, 84(1):9–18, January 2013. doi: 10.1785/0220120097.
- Michetti, A., Esposito, E., Guerrieri, L., Porfido, S., Serva, L., Tavossian, R., Vittori, E., Audemard, F., Azuma, T., Clague, J., Comerci, V., Gürpınar, A., McCalpin, J., Mohammadioun, B., Mörner, N., Ota, Y., and Roghazin, E. INQUA Environmental Seismic Intensity Scale 2007 (ESI-2007). In Guerrieri, L. and Vittori, E., editors, *Servizio Geologico d'Italia - Dipartimento Difesa del*

- Suolo. 2007.
- Molina, S., Navarro, M., Martínez-Pagan, P., Pérez-Cuevas, J., Vidal, F., Navarro, D., and Agea-Medina, N. Potential damage and losses in a repeat of the 1910 Adra (Southern Spain) earthquake. *Natural Hazards*, 92(3):1547–1571, March 2018. doi: 10.1007/s11069-018-3263-6.
- Molins-Vigatà, J., García-Mayordomo, J., Ortuño, M., García-Sellés, D., and Gómez-Novell, O. Caracterización geológica de la falla del Llano del Águila en Campo Dalías (Almería): posible fuente sismogénica del terremoto de 1804. *Revista de la Sociedad Geológica de España*, 35(1):71–83, June 2022. doi: 10.55407/rsge.94908.
- Moreno, X., Masana, E., Pallàs, R., Gràcia, E., Rodés, J. and Bordonau, J. Quaternary tectonic activity of the Carboneras Fault in the La Serrata range (SE Iberia): Geomorphological and chronological constraints. *Tectonophysics*, 663:78–94, November 2015. doi: 10.1016/j.tecto.2015.08.016.
- Moreno, X., Gràcia, E., Bartolomé, R., Martínez-Loriente, S., Perea, H., de la Peña, L. G., Iacono, C. L., Piñero, E., Pallàs, R., Masana, E., and Dañoibeitia, J. J. Seismostratigraphy and tectonic architecture of the Carboneras Fault offshore based on multiscale seismic imaging: Implications for the Neogene evolution of the NE Alboran Sea. *Tectonophysics*, 689:115–132, October 2016. doi: 10.1016/j.tecto.2016.02.018.
- Moreno Mota, X. *Neotectonic and Paleoseismic onshore-offshore integrated study of the Carboneras Fault*. SE Iberia). Universitat de Barcelona, Eastern Betics, 2011.
- Muñoz Clares, M., Fernández Carrascosa, M., Alcolea López, M., Arcas Navarro, M., Arcas Ruiz, N., Vas, P., Cruz López, M., García Poveda, M., García Valera, M., Llamas Martínez, B., and Ruiz Llanes, A. Sismicidad histórica y documentación municipal: El caso de Lorca. *Boletín Geológico y Minero*, 123(4): 415–429, 2012.
- Murphy Corella, P. Los terremotos de Almería de 1804 en el archivo histórico nacional. *Instituto Geográfico Nacional*, 2019. <https://www.ign.es/web/libros-digitales/terremotos-almeria-1804>.
- Nocquet, J.-M. and Calais, E. Geodetic Measurements of Crustal Deformation in the Western Mediterranean and Europe. *Pure and Applied Geophysics*, 161(3):661–681, March 2004. doi: 10.1007/s00024-003-2468-z.
- Okada, Y. Internal deformation due to shear and tensile faults in a half-space. *Bulletin of the Seismological Society of America*, 82(2):1018–1040, April 1992. doi: 10.1785/bssa0820021018.
- Ortuño, M., Masana, E., García-Melendez, E., Martínez-Díaz, J., Stepancikova, P., Cunha, P. P., Sohbatí, R., Canora, C., Buylaert, J.-P., and Murray, A. S. An exceptionally long paleoseismic record of a slow-moving fault: The Alhama de Murcia fault (Eastern Betic shear zone, Spain). *Geological Society of America Bulletin*, 124(9–10):1474–1494, July 2012. doi: 10.1130/b30558.1.
- Pagani, M., Monelli, D., Weatherill, G., Danciu, L., Crowley, H., Silva, V., Henshaw, P., Butler, L., Nastasi, M., Panzeri, L., Simionato, M., and Vigano, D. OpenQuake Engine: An Open Hazard (and Risk) Software for the Global Earthquake Model. *Seismological Research Letters*, 85(3):692–702, May 2014. doi: 10.1785/0220130087.
- Palano, M., González, P. J., and Fernández, J. The Diffuse Plate boundary of Nubia and Iberia in the Western Mediterranean: Crustal deformation evidence for viscous coupling and fragmented lithosphere. *Earth and Planetary Science Letters*, 430: 439–447, November 2015. doi: 10.1016/j.epsl.2015.08.040.
- Pedrerá, A., Marín-Lechado, C., Stich, D., Ruiz-Constán, A., Galindo-Zaldívar, J., Rey-Moral, C., and de Lis Mancilla, F. Nucleation, linkage and active propagation of a segmented Quaternary normal-dextral fault: the Loma del Viento fault (Campo de Dalías, Eastern Betic Cordillera, SE Spain). *Tectonophysics*, 522–523:208–217, February 2012. doi: 10.1016/j.tecto.2011.12.001.
- Perea, H. The Catalan seismic crisis (1427 and 1428; NE Iberian Peninsula): Geological sources and earthquake triggering. *Journal of Geodynamics*, 47(5):259–270, May 2009. doi: 10.1016/j.jog.2009.01.002.
- Perea, H., Gràcia, E., Martínez-Loriente, S., Bartolome, R., de la Peña, L. G., de Mol, B., Moreno, X., Iacono, C. L., Diez, S., Tello, O., Gómez-Ballesteros, M., and Dañoibeitia, J. J. Kinematic analysis of secondary faults within a distributed shear-zone reveals fault linkage and increased seismic hazard. *Marine Geology*, 399: 23–33, May 2018. doi: 10.1016/j.margeo.2018.02.002.
- Perea, H., Roldán, J., Sánchez-Lozano, L., Álvarez Gómez, J., Herrero-Barbero1, P., Jiménez4, M., Martínez-Loriente2, S., C., A., and L, J. Serie sísmica del sur del Mar de Alborán del 2021-2022: relocalización de los eventos e implicaciones sismotectónicas. In *IV Reunión Ibérica Sobre Fallas Activas y Paleosismología*, page 141–144. 2022.
- Pezeshk, S., Zandieh, A., Campbell, K. W., and Tavakoli, B. Ground-Motion Prediction Equations for Central and Eastern North America Using the Hybrid Empirical Method and NGA-West2 Empirical Ground-Motion Models. *Bulletin of the Seismological Society of America*, 108(4):2278–2304, June 2018. doi: 10.1785/0120170179.
- Posadas, A., Vidal, F., and Navarro, M. The M = 6.3 Earthquake of January 13 (1804) in Motril (Spain). In *Proceedings of the First European Conference on Earthquake Engineering and Seismology*, volume 91, page 1–8, 2006.
- Quirós Hernández, L. E. *Modelizaciones y análisis de sensibilidad en la evaluación integral del riesgo sísmico a escala urbana. Aplicación a la ciudad de Lorca*. Tesis doctoral, Universidad Politécnica de Madrid, Escuela Técnica Superior de Ingenieros Industriales, Madrid, España, 2017. Ingeniería sísmica: Dinámica de suelos y estructuras.
- Rodríguez-Pascua, M., Silva, P., Perucha, M., Robles, J., Elez, J., and Roquero, E. El escenario sísmico del terremoto de Arenas del Rey de 1884. In *IX Reunión Do Quaternário Ibérico*, page 49–52. 2017.
- Sanz de Galdeano, C., Azañón, J. M., Cabral, J., Ruano, P., Alfaro, P., Canora, C., Ferrater, M., García Tortosa, F. J., García-Mayordomo, J., Gràcia, E., Insua-Arévalo, J. M., Jiménez Bonilla, A., Llacan, P. G., Marín-Lechado, C., Martín-Banda, R., Martín González, F., Martínez-Díaz, J. J., Martín-Rojas, I., Masana, E., and ... Simón, J. L. *Active faults in Iberia*, pages 33–75. Cambridge University Press, Cambridge, 2020.
- Sanz de Galdeano, C. S., Rodríguez-Fernandez, J., and Lopez-Garrido, A. C. A strike-slip fault corridor within the Alpujarra Mountains (Betic Cordilleras, Spain). *Geologische Rundschau*, 74(3):641–655, October 1985. doi: 10.1007/bf01821218.
- Serpelloni, E., Vannucci, G., Pondrelli, S., Argnani, A., Casula, G., Anzidei, M., Baldi, P., and Gasperini, P. Kinematics of the Western Africa-Eurasia plate boundary from focal mechanisms and GPS data. *Geophysical Journal International*, 169(3):1180–1200, June 2007. doi: 10.1111/j.1365-246x.2007.03367.x.
- Silva, P., Goy, J., Somoza, L., Zazo, C., and Bardají, T. Landscape response to strike-slip faulting linked to collisional settings: Quaternary tectonics and basin formation in the Eastern Betics, southeastern Spain. *Tectonophysics*, 224(4):289–303, September 1993. doi: 10.1016/0040-1951(93)90034-h.
- Silva, P., Elez, J., Giner-Robles, J., Rodríguez-Pascua, M., Pérez-López, R., Roquero, E., Bardají, T., and Martínez-Graña, A. ESI-07 ShakeMaps for instrumental and historical events in the Betic Cordillera (SE Spain): An approach based on geological data

- and applied to seismic hazard. *Quaternary International*, 451: 185–208, September 2017. doi: 10.1016/j.quaint.2016.10.020.
- Silva, P. G., Elez, J., Pérez-López, R., Giner-Robles, J. L., Gómez-Diego, P. V., Roquero, E., Rodríguez-Pascua, M. X and Bardaji, T. The AD 1755 Lisbon Earthquake-Tsunami: Seismic source modelling from the analysis of ESI-07 environmental data. *Quaternary International*, 651:6–24, March 2023. doi: 10.1016/j.quaint.2021.11.006.
- Stein, R. S. The role of stress transfer in earthquake occurrence. *Nature*, 402(6762):605–609, December 1999. doi: 10.1038/45144.
- Stein, R. S. Earthquake Conversations. *Scientific American*, 288(1): 72–79, January 2003. doi: 10.1038/scientificamerican0103-72.
- Stirling, M., Rhoades, D., and Berryman, K. Comparison of Earthquake Scaling Relations Derived from Data of the Instrumental and Preinstrumental Era. *Bulletin of the Seismological Society of America*, 92(2):812–830, March 2002. doi: 10.1785/0120000221.
- Stirling, M., Litchfield, N., Villamor, P., Dissen, R., Nicol, A., Pettinga, J., Barnes, P., Langridge, R., Little, T., Barrell, D., Mountjoy, J., Ries, W., Rowland, J., Fenton, C., Hamling, I., Asher, C., Barrier, A., Benson, A., Bischoff, A., and Zinke, R. The M(w)7.8 2016 Kaikoura earthquake: surface fault rupture and seismic hazard context. *Bulletin of the New Zealand Society for Earthquake Engineering*, 50(2):73–84, 2017.
- Teves-Costa, P. and Batlló, J. The 23 April 1909 Benavente earthquake (Portugal): macroseismic field revision. *Journal of Seismology*, 15(1):59–70, October 2010. doi: 10.1007/s10950-010-9207-6.
- Toda, S., Stein, R. S., Sevilgen, V., and Lin, J. *Coulomb 3.3 Graphic-rich deformation and stress-change software for earthquake, tectonic, and volcano research and teaching-user guide*. 2011. doi: 10.3133/ofr20111060.
- Trifunac, M. and Brady, A. On the correlation of seismic intensity scales with the peaks of recorded strong ground motion. *Bulletin of the Seismological Society of America*, 65(1):139–162, 1975.
- Tselentis, G.-A. and Danciu, L. Empirical Relationships between Modified Mercalli Intensity and Engineering Ground-Motion Parameters in Greece. *Bulletin of the Seismological Society of America*, 98(4):1863–1875, August 2008. doi: 10.1785/0120070172.
- Wald, D. J., Quitoriano, V., Heaton, T. H., and Kanamori, H. Relationships between Peak Ground Acceleration, Peak Ground Velocity, and Modified Mercalli Intensity in California. *Earthquake Spectra*, 15(3):557–564, August 1999. doi: 10.1193/1.1586058.
- Wells, D. L. and Coppersmith, K. J. New empirical relationships among magnitude, rupture length, rupture width, rupture area, and surface displacement. *Bulletin of the Seismological Society of America*, 84(4):974–1002, August 1994. doi: 10.1785/bssa0840040974.
- Worden, C. B., Gerstenberger, M. C., Rhoades, D. A., and Wald, D. J. Probabilistic Relationships between Ground-Motion Parameters and Modified Mercalli Intensity in California. *Bulletin of the Seismological Society of America*, 102(1):204–221, February 2012. doi: 10.1785/0120110156.

The article *The 1804 Alborán Seismic Series: Search for the Source* © 2025 by Yolanda de Pro-Díaz is licensed under CC BY 4.0.